Fluidised-Bed Chlorination of Oxidised Titania Slag.

By

BUNGU PETER NDULA

A dissertation submitted in fulfilment of the requirements for the degree

MASTER OF SCIENCE (METALLURGY)

in the

Faculty of Engineering, the Built Environment and Information Technology

University of Pretoria

2004

Fluidised-Bed Chlorination of Oxidised Titania Slag.

STUDENT : BUNGU PETER NDULA

SUPERVISOR : P.C. PISTORIUS

DEPARTMENT : MATERIAL SCIENCE AND METALLURGICAL ENGINEERING.

DEGREE : MASTER OF SCIENCE (METALLURGY)

ABSTRACT

High-titanium slag (produced by carbothermic reduction of ilmenite) contains a significant percentage of trivalent titanium, which can be converted to the tetravalent form by oxidation. Oxidation can occur through contact with water vapour, for example during water granulation. This work investigated the degree of oxidation of the different size fractions of water granulated titania slag, and the resultant changes in phase composition. For this oxidised slag, the kinetics and exothermicity of the chlorination process are also reported.

Key words

Oxidised titania slag, water granulation, M_3O_5, anatase, rutile, chlorination, block route slag.

ACKNOWLEDGEMENTS

I wish to express my sincere thanks and appreciation to my supervisor, Professor P.C Pistorius for his constant advice, guidance and direction throughout this research work. I remain indebted to Kumba Resources for their support and sponsorship and the Innovation Fund awarded by the Department of Arts, Culture, Science and Technology.

My appreciation also goes to Professor T.A. Modro, the former head of Chemistry department and Zsussana Foldvari for their motivation, inspiration and support in pursuing studies in the University of Pretoria. Special thanks go to the following:

Late Mr. Johann Borman for his technical assistance, Sarah Havenga for her support, Sabine Verryn for assistance with the XRD analyses, Carl Coetzee for his assistance with the SEM work, Peter Sibiya for polishing the SEM samples, Deon Bessinger for the XRF analyses, and fellow pyrometallurgical students, Daudet T, Ulyate, Mutale and Tomi for their support and advice. The assistance of Giovanni Hearne and Antoine Mulaba (who performed the Mössbauer measurements and analyses) is also gratefully acknowledged.

I wish also to thank my Uncle Pa Lambi Umaru Kumsike for initiating my academic career and my wife Bungu Florence Kuvin for moral support and my daughter Bungu Tracey Ikeh for inspiring me to work harder. Finally, my special thanks go to the Almighty God for providing me with the wisdom, good health, and strength in successfully completing the programme.

DEDICATION

The research work is dedicated to my beloved late mother, Late Ma Ikeh Agnes Ndula who supported me from birth and died on the 30th of August 1994. May her soul rest in peace.

TABLE OF CONTENTS

LIST OF FIGURES

LIST OF TABLES

1 INTRODUCTION

1.1 Background and Main Objectives of the Project.

The first recorded use of titanium dioxide as a white pigment was in 1908 when A.J. Rossi, a French metallurgist and chemist who had come to the United States in the late 1800s, mixed the material with salad oil and brushed out the mixture (Fisher, 1997). Work continued in the United State on the use of titanium dioxide as pigment and in 1916 a Titanium Pigment Company was formed in Niagara Falls, New York (Fisher, 1997). Titanium is the ninth most abundant element in the earth's crust and the fourth most abundant metallic element (Minkler and Baroch, 1981). Rutile is traditionally the feedstock of choice used in the production of white pigment and is the main or primary source of all forms of titanium concentrates in the pigment industry. Except for sulphate route pigment production, which is becoming increasingly less prevalent in the face of environmental concerns, (Minkler and Baroch, 1981) the chloride route pigment and titanium metal producers all use the same intermediate, $TiCl_4$. The titanium tetrachloride must be of high purity. Titanium sponge is also produced from $TiCl_4$ generated by the pigment producers (Minkler and Baroch, 1981).

Titania slag, a product of the reductive smelting of ilmenite ($FeO.TiO_2$), plays an increasingly important role as feedstock in the production of TiO_2 pigment by the sulphate or chloride routes. This is due to the rising price and limited resources of natural rutile (Sohn and Zhou, 1998). In the smelting of ilmenite at approximately 1650-1700^{O}C, the iron content of the slag phase is decreased by a suitable carbonaceous reductant in an electric furnace to produce high titania slag as the major product. In the process, pig iron is produced as by-product (Kahn, 1983). It was found that, where high titania slag does not undergo oxidation upon tapping, there was a parallel reduction of FeO to Fe and TiO_2 to Ti_2O_3 during the ilmenite smelting process. The partial reduction of TiO_2 does not contribute to upgrading of the slag, however, the formation of Ti_2O_3 does have a beneficial effect of lowering the liquidus temperature of the slag, (Pistorius, 2002).

According to (Bessinger et al, 1997), there are four phases present in high titania slags with pseudobrookite (M_3O_5 solid solution) being the most common phase. The amount of the other phases varies from slag to slag, depending on the chemistry of the slag as well as the conditions under which each slag had been cooled. Chlorinatable high titania slag typically contains about 10%FeO, 52%TiO_2 and 33%Ti_2O_3 (with other impurities mainly SiO_2, CaO, MgO, and Al_2O_3), making up the balance (Bessinger et al, 1997).

The slag used in this work was produced by carbothermic reduction of ilmenite to form titania slag. Upon tapping, a high-pressure water jet was use to disintegrate the slag into fragments. As a result of this, the slag cooled down much faster than the block route slag. This technique of slag granulation is attractive since it avoids the long cooling time associated with slag ingots and eliminates several crushing steps. A concern is that the slag may react with water or oxygen during tapping and become oxidized. On the other hand, the block route slag used in the project (abbreviated as BSC), which was less oxidized, was produced by collecting the liquid slag in a ladle and allowing this to cool slowly. The cooled ingots were then crushed and milled to yield the size fractions required for the chlorination process. The typical size range is larger than 100μm and smaller than 850μm. The particle size range used in this work was 425-600μm.

The first purpose of this project was to identify and quantify the different phases present in the oxidized titania slag, and to investigate the microscopic nature, the amount of each phase present and the phase changes that occur during the first few minutes of chlorination of the oxidised slag as compared to that of unoxidised block route slag.

In addition to changing the phase composition, oxidation of the slag changes the energy balance during chlorination. The typical temperature used in industrial chlorination is 1223K to avoid sintering of the bed (Zhou et.al. 1996). The presence of Ti^{3+} in the slag contributes to heat evolved in the chlorinator that could cause the fluidized bed to sinter. This is because the chlorination reaction of Ti^{3+} is highly exothermic (Minkler and Baroch, 1981). Pistorius and le Roux,

(2002) also concluded that slag chlorination was exothermic due to the presence of Ti_2O_3 and therefore will produce heat in the fluidized-bed. For this reason, titania slag must have a Ti_2O_3 content of less than 25% (Minkler and Baroch, 1981).

Chlorination of FeO and other impurity oxides, like MnO, occurs within the first few minutes of the process thereby creating porosity in the slag matrix. The porosity created had a significant role on the chlorination kinetics of the slag. (Sohn and Zhou, 1998 ; Pistorius and le Roux, 2002). If the slag oxidises during or after tapping, some of the Ti^{3+} is transformed to Ti^{4+}, and upon more extensive oxidation Fe^{2+} is transformed to Fe^{3+}. In this case, the solidified slag contains both titanium and iron in the +4 and+3 oxidation states respectively hence changing the composition of the slag significantly. The resulting changes in phase composition will in turn reduce the porosity of the slag matrix (due to the slow chlorination rate of Ti and Fe in their highest oxidation states) and hence slowing down the overall rate of reaction. The behaviour of the slag during chlorination in the fluidized-bed reactor would be a good quality control test for the slag (le Roux, 2001). For these reasons, the second purpose of this project was to study the effect of slag oxidation on the chlorination kinetics of the slag.

2 LITERATURE SURVEY

2.1 Properties and Uses of Titanium Metal and Its Oxides.

Titanium dioxide reflects and scatters light in the visible spectrum like thousands of tiny mirrors. This means that, when it is incorporated in paints, plastics or paper, it imparts brilliance and opacity to these products (Minkler and Baroch, 1981; Richards Bay Minerals). Unlike poisonous lead compounds, which may also be used to give the white and bright colour, TiO_2 is non-poisonous, non-toxic, and biologically inert. TiO_2 absorbs the dangerous ultraviolet (UV) rays from the sun, hence it is used in modern sunscreen to prevent skin cancer. Rutile is also used in welding rod fluxes. It stabilizes the arc and protects the molten metal from oxidation during welding, hence forming a superior welding joint (Richards Bay Minerals; Fisher, 1997). It is also used in certain metallurgical and electronic applications and extensively in surface coatings (Fisher, 1997). Finally, it is used in the manufacture of titanium metal. Due to the excellent properties of the metal (lightness, strength, corrosion resistance and heat resistance) it is used extensively in the aerospace industries. The lightness, strength and inert properties make it ideal for use in artificial hip joints, heart pace makers and spectacle frames (Minkler and Baroch, 1981; Richards Bay Minerals).

2.2. Titaniferous Feedstocks.

2.2.1. Feedstocks for the production of titanium tetrachloride.

The decision on which route to follow in transforming titanium ore (or upgraded ilmenite) to the pigment will depend on the purity level of the feedstock. The sulphate route has been used to process lower grade titanium feedstock. The chloride process requires significantly higher-grade titanium feedstock (van Dyk et al. 1999). This work will focus on titania slag produced from South Africa ilmenite with low impurity content. These impurities (such as MnO, MgO, CaO, Al_2O_3, and SiO_2) largely report to the slag, making up about 6% (by mass) of the total (Pistorius, 2002).

There are still large deposits of rutile in a limited number of places such as Australia, Sri Lanka, South Africa, India and Sierra Leone (Minkler and Baroch, 1981; van Dyk et. al. 1999). However, the price of rutile has quadrupled over the last twenty years. This resulted in a shift towards the use of substitute materials for natural rutile. Other abundant low-grade titanium minerals such as ilmenite ($FeTiO_3$), arizonite ($Fe_2O_3.nTiO_2.mH_2O$), leucoxene ($Fe_2O_3.nTiO_2$), perovskite ($CaTiO_3$) and titaniferous magnetite must be utilized as substitutes for rutiles. In South Africa, Richard Bay Minerals obtains its rutile and ilmenite from the coastal area of northern Kwazulu-Natal along the Zululand coast (Richards Bay Minerals). Namakwa Sands, which is an Anglo American company, uses a direct electric arc furnace in the smelting of ilmenite obtained from mineral sands on the western coast.

Due to the high level of impurities - especially iron - in these minerals, it is necessary to upgrade them to obtain synthetic rutile or other high-titanium feedstocks, which are acceptable for chlorination (Rhee and Sohn, 1990). High quality titania slag is also used in pigment production as a substitute for natural rutile. A number of processes have been proposed for the removal of iron from low-grade titanium ore (Minkler and Baroch, 1981). Typical compositions of rutile, ilmenite and high titania slag are given in table 2.2.

Table 2.2: Typical Composition Of Rutile, Ilmenite and High Titania Slag (Kahn, 1983; Minkler and Baroch, 1981)

Compounds	Rutile (USA) % by weight	Ilmenite (USA) % by weight	High titania slag (RBM) % by weight	Synthetic rutile (Western) % by weight
TiO_2	96.06[a]	64.6[a]	85.5[a]	92.8[a]
Ti_2O_3	-	-	25.0	10.0
Fe_2O_3	1.46	29.8	-	-
FeO	-	-	7.5	-
Fe (metallic)	-		0.2	
Fe (total)		20.8		2.1
MnO	-	-	1.4	1.0
Al_2O_3	0.33	0.62	2.0	1.1
SiO_2	-	0.26	1.5	1.2
ZrO_2	0.05	0.027	-	0.15
V_2O_5	-	0.22	0.40	0.02
Cr_2O_3	0.08	-	0.22	0.03
NbO_3	-	-	-	0.2
MgO	0.038	0.2	0.9	0.3
CaO	0.034	0.086	0.14	0.03
P_2O_5	0.09	0.16	-	0.02
C	-	-	0.07	0.3
S	-	-	0.06	0.3

a TiO_2 actually gives the total titanium content, expressed as TiO_2 (i.e. including both trivalent and tetravalent titanium).

2.2.2 Characterization Of Chlorinatable Titaniferous Feedstock

Environmental pressures on waste disposal are forcing pigment producers to use feedstocks with a higher content of TiO_2 and lower levels of trace elements. Manufacturers who use ilmenite directly once enjoyed a cost advantage. Nowadays this advantage is diminishing because of environmental concerns arising from the fact that a larger amount of iron waste product is generated from direct ilmenite use (Stanaway, 1994). Because the sulphate process produces

up to three times more waste than the chloride process, more effort now goes to supply the chloride producers where a volume growth of 40% is expected over the next 10 years (Stanaway, 1994). Recently, the demand for chlorinatable upgraded ilmenite (synthetic rutile), has began to rival that of natural rutile (van Dyk et. al. 1999). Pistorius and le Roux, (2002) reported that titania slag with 86.45-89.38mass% TiO_2 could also be chlorinated effectively.

2.2.3 Techniques for the Upgrading of Sub-Rutile feedstocks.

Due to ilmenite's wide geological distribution and price advantage over rutile, hundreds of techniques have been proposed for upgrading the TiO_2 content in ilmenite making it a more feasible feedstock for the generation of $TiCl_4$ (Minkler and Baroch, 1981; Kahn, 1983). Four main routes to the successful production of synthetic rutile from ilmenite are shown in figure 2.2.3 below (Kahn, 1983).

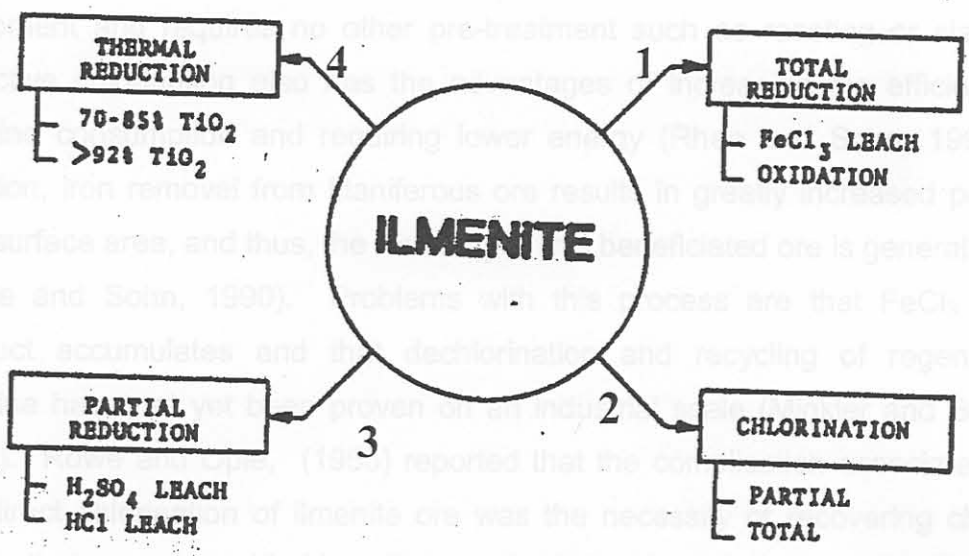

Figure 2.2.3: Possible Ilmenite to Rutile Routes (Kahn, 1983)

Route 1 is the Becher process, which involves a pre-oxidation step followed by total reduction of the ilmenite to metallic iron by coal in a rotary kiln (Minkler and Baroch, 1981; Kahn, 1983). The iron is then removed by agitating the metallized

ore in aerated water in the presence of a catalyst (NH_4Cl). The iron is oxidised and then separated from the leached ilmenite in a washing cyclone (Kahn, 1983). TiO_2 is acid leached to removed the ferrous oxide and dried to yield synthetic rutile (Minkler and Baroch, 1981). The leaching typically proceeds for 12-16 hours at 70-80^{o}C.

Route 2, known as the Dunn process, is based on the fact that iron in ilmenite chlorinates selectively and more readily than titanium. After pre-treatment, the ore is chlorinated in a fluidized-bed with an excess of ilmenite so that any titanium that chlorinates will react with the iron oxide and remain in the concentrate as TiO_2. The iron chloride gas leaving the bed is reacted with oxygen to form iron oxide and chlorine gas for recycling (Minkler and Baroch, 1981) and (Kahn, 1983). Under proper conditions, iron extraction is essentially complete before $TiCl_4$ production commences. Direct chlorination has a significant advantage in that it could be done in conventional chlorination equipment and requires no other pre-treatment such as roasting or slagging. Selective chlorination also has the advantages of increasing the efficiency of chlorine consumption and requiring lower energy (Rhee and Sohn, 1990). In addition, iron removal from titaniferous ore results in greatly increased porosity and surface area, and thus, the reactivity of this beneficiated ore is generally high (Rhee and Sohn, 1990). Problems with this process are that $FeCl_3$ waste product accumulates and that dechlorination and recycling of regenerated chlorine have not yet been proven on an industrial scale (Minkler and Baroch, 1981). Rowe and Opie, (1955) reported that the complication associated with the direct chlorination of ilmenite ore was the necessity of recovering chlorine values tied up as iron chlorides. Direct oxidation of $FeCl_3$ was not efficient, owing to its tendency to dissociate into the difficultly oxidisable $FeCl_2$. Other operational difficulties associated with the chlorination of titaniferous feedstocks are the defluidization and clogging caused by high-boiling point metal chlorides produced during chlorination (Rhee and Sohn, 1990). Nonetheless, these difficulties can be alleviated by the control of temperature, amount of reducing

agent and the partial pressure of chlorine. Another type of direct chlorination of the ore is the chlorination of both iron and titanium, forming volatile chlorides, which are subsequently separated (Rhee and Sohn, 1990).

Route 3, which is the Benelite process (Minkler and Baroch, 1981; Kahn, 1983), involves partial reduction of ilmenite with carbonaceous material in a rotary kiln, converting the ferric oxide (Fe_2O_3) to ferrous oxide (FeO). The reduced ilmenite is cooled and charged into a digester for leaching with 18-20% hydrochloric acid at 140^{O}C to give beneficiated ilmenite (synthetic rutile).

Route 4 is a viable approach and is usually performed by electric arc furnace smelting of ilmenite to produce pig iron and high titania slag. The product, high titania slag can be converted to a white pigment through the chloride route, (Kahn, 1983). This project deals with the chlorination of such high titania slag.

2.3 Oxidation of High Titania Slag.

Because of the presence of trivalent titanium in high-titanium slag, the slag can undergo oxidation in the solid state, as shown by various studies.

Borowiec et. al. (1998) developed a method to upgrade several types of titania slag such as Sorelslag^{TM} with total Ti content (reported as TiO_2) in the range 78.30-84.80 weight % and Richards Bay slag of composition 86.20 weight % TiO_2. These slags are sized to a particle size range of 75-850 microns, and oxidised with an oxygen containing gas at a temperature of at least about 950^{O}C for at least 20 minutes. During this process, a substantial portion of the iron oxide and Ti_2O_3 are converted to the ferric and TiO_2 states respectively and the glassy silicate phase decomposes. The oxidised slag is then reduced at a temperature of at least 700^{O}C such that the ferric oxides are again converted to the ferrous state. The product is then leached with 20% excess of mineral acid at a temperature of at least 125^{O}C and one atmospheric pressure to yield the upgraded slag. The slag is then washed and calcined by heating to a

temperature in the range 600-800^{O}C. The product contains TiO_2 content in the range 93-96 wt %.

Vasyutinsky and Movsesov, (1965) studied the oxidation and grinding of titania slag containing 90.1%TiO_2 and 3.47%FeO. They concluded that to obtain the maximum reduction in strength of the slag, oxidation of the slag in the temperature region of 500-600^{O}C was required. Vasyutinsky, (1968) did an in-depth study of the oxidation of a similar high titania slag. The slag consisted mainly of a M_3O_5 phase, which could best be represented as x[(Fe, Mg, Mn)O. $2TiO_2$].y[(Ti, Al, Cr)$_2O_3$.TiO_2 solid solution. The experimental results on the oxidation of the slag indicated the following three main stages:

- At temperature of approximately 300-400^{O}C, only structural changes in the M_3O_5 phase was observed. X-ray diffraction analysis indicated a distortion of the M_3O_5 crystal lattice.
- At temperature $\leq$ 750^{O}C, the formation of anatase was observed.
- At higher temperature the formation of rutile was observed.

The anatase to rutile conversion temperature can range between 400-1000^{O}C, depending on the source of the anatase and type of impurities in it.

Bessinger et al. (2001) studied the decrepitation of solidified high titania slag. This was done by oxidising titania slag samples produced in a pilot plant furnace at temperature between 400 and 800^{O}C. During the slag cooling process, severe decrepitation of the slag may occur. This was detrimental to the slag because an excess of fine materials with average particle diameter of less than 106μm was produced. This lower valued products should be minimized in order to maximize the income that could be derived from titania slag. Decrepitation is defined as the disintegration or crumbling of a material into component parts or smaller fragments. Generally, decrepitation of slags occur due to phase and chemical changes in the slag and resultant volume changes associated with these phase changes, (Noguchi et al.,1980). Decrepitation of high titania slags was explained by oxidation of the M_3O_5 phase, resulting in the formation of anatase. As the density of anatase is less than the density of the M_3O_5 phase, this resulted in cracking of the slag (Vasyutinsky, 1968). Bessinger et al. (2001) confirmed that

decrepitation of titania slags was observed after heating at 400°C. They postulated that decrepitation occurs due to changes in the crystal lattice of the M_3O_5 phase in the slag due to oxidation .

2.4. Mineralogy and Phase Chemistry Of Titaniferous Feedstock

Ilmenite refers to the compound $FeTiO_3$, but naturally occurring ilmenite can also contain small amounts of MnO, MgO, Fe_2O_3 or Ti_2O_3 in its structure (van Dyk et al. 1999). As mentioned in section 1.1, four main mineralogical phases were identified to be present in the various high-titanium slags (Bessinger et al. 1997). The major phase is a solid solution phase referred to as M_3O_5 with end-members of the solid solution series such as $FeTi_2O_5$ (ferropseudobrookite), $MgTi_2O_5$ (armalcolite), and Ti_3O_5 (anosovite). The other three phases are rutile, metallic iron and a glassy phase (Bessinger et. al. 1997; Nell, 1999).

Table 2.4: Chemical Composition of Various Upgraded Titaniferous Feedstocks (van Dyk et al. 1999).

	TiO_2	FeO	MgO	Al_2O_3	CaO	V_2O_5	Cr_2O_3	MnO	SiO_2
Titania slag	86.4	10.5	1.00	1.00	0.13	0.42	0.11	1.71	1.58
Upgraded slag	94.9	2.47	0.67	0.46	0.06	0.35	0.06	0.03	1.69
Benelite synthetic rutile	93.8	4.83	0.02	0.51	0.05	0.08	0.02	0.05	1.34
Becher synthetic rutile	95.1	2.65	0.35	1.12	0.05	0.27	0.12	0.71	0.95

Van Dyk et al. (1999) reviewed the properties of some upgraded feedstocks, table 2.4. Of these, the feedstock with lowest TiO_2 content (86 %) and the highest impurity level was titania slag. The TiO_2 content of the other main feedstocks ranged between 93-95%. The main impurity in all the products was iron (as iron oxide). The levels of minor impurities in the product were all below

the levels specified for the chloride process, although the silica content in the titania slag and upgraded slag products may be too high for some chloride plants (van Dyk et al. 1999). As stated before, the slag consisted primarily of M_3O_5 (pseudobrookite) phase together with trace amounts of rutile. The Benelite synthetic rutile and upgraded slag products both have rutile as the main phase, with M_3O_5 present as trace phase. In the Becher synthetic rutile, Ti_3O_5 was the main phase along with rutile. M_3O_5, ilmenite and metallic iron were also present as minor and trace components (van Dyk et al. 1999). The trivalent titania (Ti_2O_3) occurs as a result of the highly reducing conditions applied in the Becher process to reduce all of the iron oxide to the metallic state. The M_3O_5 phase in the titania slag particles had a dense appearance and smooth texture.

2.4.1 Ti-O-Fe Phase diagram

A continuous solid solution series exists between $Fe_2^{3+}Ti_2O_5$ (ferripseudobrookite), $Fe^{2+}Ti_2O_5$ (ferropseudobrookite) and $Ti^{4+}Ti_2^{3+}O_5$ or Ti_3O_5 (anosovite) at temperatures above 1320^{O}C. The end members of these solid solutions are unstable at low temperatures. As reported by Eriksson et. al. (1996), ferripseudobrookite decomposes to rutile and hematite below 585-/+5^{O}C, while ferropseudobrookite decomposes below 1140+/-10^{O}C to rutile and ilmenite.

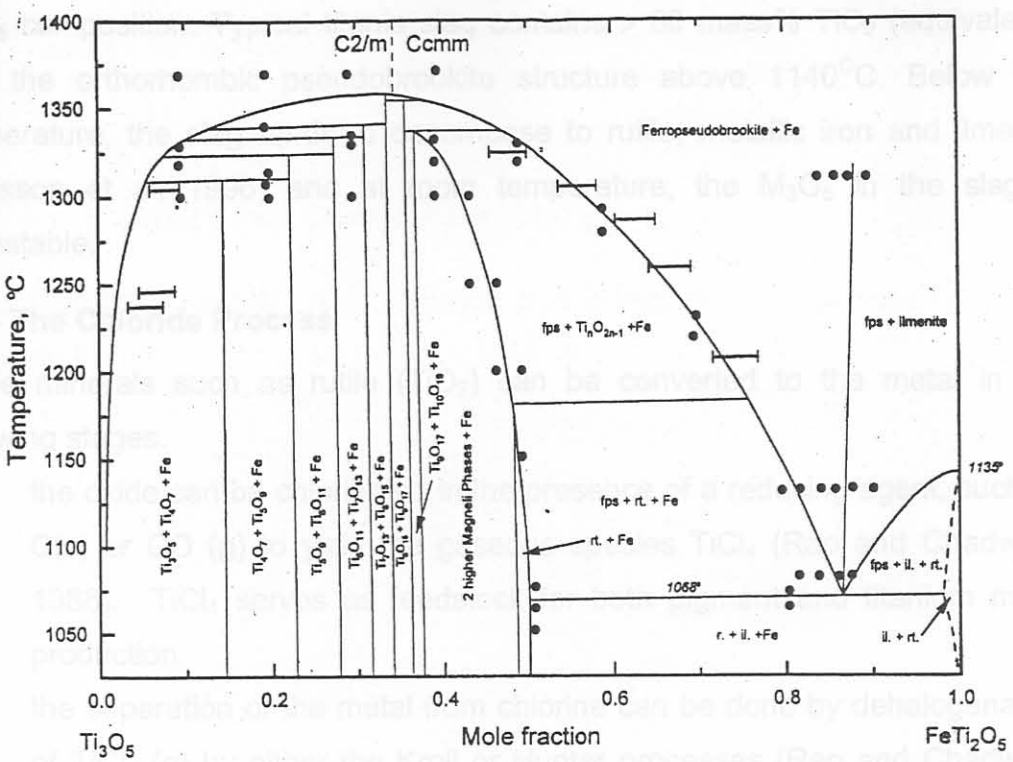

Figure 2.4.1: Binary Section $FeTi_2O_5$-Ti_3O_5 through The Fe-Ti-O Phase Diagram (Eriksson et al. 1996)

Eriksson et al. (1996) investigated the stability of pseudobrookite type solid solutions in the binary section $FeTi_2O_5$-Ti_3O_5 of the Fe-Ti-O phase diagram. They found that, towards higher titanium concentrations, the solid solution based on Ti_3O_5 decomposes below the solvus line to give a series of Magneli phases as seen in figure 2.4.1. These Magneli phases have the general formula Ti_nO_{2n-1} where $4 \leq n \leq 10$. (Eriksson et al. 1996).

These series of solid solution were also studied by Grey et al. (1973) for variations in temperature and oxygen partial pressure. They found that the solid solution was complete at temperatures above 1350°C. For the series $Fe_xTi_{3-x}O_5$ (with $0 \leq x \leq 1$) it was found that with $x > 0.35$ the compounds have an orthohombic pseudobrookite structure. With $x < 0.35$ the compounds have a monoclinic distortion of this structure, with the distortion increasing towards the

Ti_3O_5 composition. Typical titania slag contains > 80 mass% TiO_2 (equivalent), with the orthorhombic pseudobrookite structure above 1140^{O}C. Below this temperature, the slag tends to decompose to rutile, metallic iron and ilmenite (Eriksson et al. 1996) and at room temperature, the M_3O_5 in the slag is metastable.

2.5 The Chloride Process

Oxide minerals such as rutile (TiO_2) can be converted to the metal in the following stages.

i. the oxide can be chlorinated in the presence of a reducing agent, such as C(s) or CO (g) to yield the gaseous species $TiCl_4$ (Rao and Chadwick, 1988). $TiCl_4$ serves as feedstock for both pigment and titanium metal production.

ii. the separation of the metal from chlorine can be done by dehalogenation of $TiCl_4$ (g) by either the Kroll or Hunter processes (Rao and Chadwick, 1988), reactions 2.5a and b.

$TiCl_{4\,(g)} + 2Mg_{\,(l,\,g)} \rightarrow Ti_{(s)} + 2MgCl_{2\,(l)}$ (Kroll process) ----------2.5a.

$TiCl_{4(g)} + 4Na_{(l,g)} \rightarrow Ti_{(s)} + 4NaCl_{(l)}$ (Hunter Process)----------2.5b.

iii. The titanium sponge can then be purified by high temperature distillation under vacuum or by an inert-gas sweep. The residual salts can also be removed by the leaching of the sponge (Rao and Chadwick, 1988).

2.5.1 Fluidized Bed Reactor

A fluidised bed reactor was used in this project for the chlorination of oxidized titania slag, hence the underlying principle of the reactor is discussed below.

In the reactor, a bed of finely divided solids is lifted and agitated by a rising stream of gas or liquid. At low gas velocities, the lifting effect of the bed is slight and the system behaves like a boiling liquid. With increasing velocity, the

proportion of particles entrained in the gas stream also increases until at some point the gas carries away all particles fed into the bed (Szekely and Themelis, 1971).

2.5.1 i Fluid Flow Through Packed Beds

The simplest representation of a packed bed is that of a vertical tube filled with particles of a uniform size; see Fig 2.5.1 below.

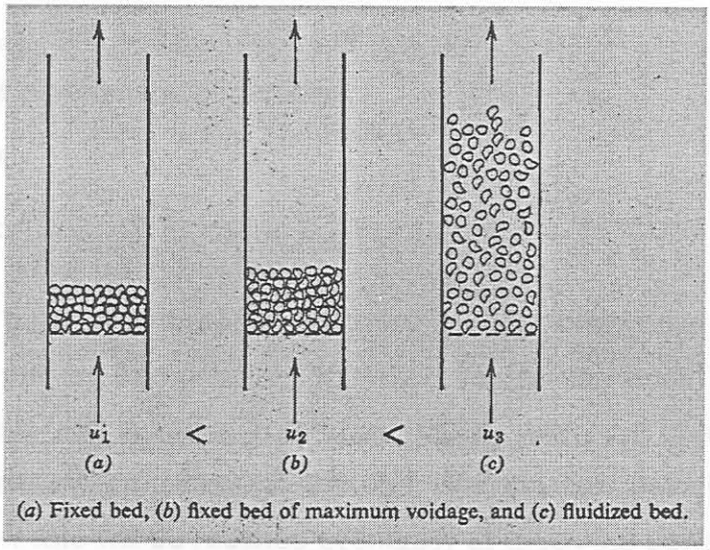

(a) Fixed bed, (b) fixed bed of maximum voidage, and (c) fluidized bed.

Fig 2.5.1: a.) Fixed bed, b.) Fixed bed of maximum voidage, c.) Fluidized bed (Szekely and Themelis, 1971).

The constitution of the bed is characterized by the following parameters: void fraction or voidage (ε), particle size and particle shape factor,

Where Voidage (ε) = (total volume of bed – volume of solid particles)/total volume of bed. ----------2.5.1a

The size of a nonspherical particle may be expressed in terms of the volume equivalent diameter defined as,

d_p = diameter of a sphere of equal volume to particle (cm). ---- 2.5.1b

For solids of irregular shape but exhibiting roughly spherical symmetry, the mesh size determined by sieving is a good approximation of the equivalent volume

diameter. However, in many cases, it is necessary to define the deviation of the shape of a particle from a sphere quantitatively, by mass of a correction factor, which is called the shape factor (Φ_s) given as

Φ_s = Surface area of sphere of equal volume to particle/Surface area of particle. ----------2.5.1c

For spherical particles;

Φ_s =1

for other shape of particle;

Φ_s < 1.

2.5.1 ii Fluid Flow in Fluidized Beds

The nature of fluidization may be illustrated by considering the upward flow of gas through a packed bed of solid, Figure 2.5.1a (Szekely and Themelis, 1971). At low flow rates, any increase in the gas velocity will result in a corresponding increase in pressure drop through the bed. As the fluid velocity is increased gradually, a flow rate will be reached eventually at which the upward force due to the pressure drop across the bed is equal to the weight of the particles in the bed. At this stage, the particles become rearranged so as to offer less resistance to fluid flow and the bed expands, Figure 2.5.1 b. The expansion continues with further increase in gas velocity, until the bed assumes the loosest possible packing. At even higher gas velocity, the particles become freely suspended in the gas stream. Under these conditions, the bed is said to be in a fluidized state, Fig 2.5.1 c. From a macroscopic point of view, a gas-solid fluidized bed may be regarded as a well stirred, boiling liquid. Because of the high degree of mixing of the solids, it is relatively easy to maintain uniform temperatures within the bed. This ready control of temperature, plus the facility of handling the solid feed and product as pseudofluids, has resulted in the wide use of fluidized beds as reactors for highly exothermic and endothermic reactions (Szekely and Themelis, 1971).

2.5.1 iii Minimum and Maximum Fluidization Velocity

The minimum fluidization velocity denoted U_{mf} is the velocity at which the pressure drop across the bed is equal to the weight of the solid particles. It is derived from the following:

$$A_B g\Delta P = A_B L_{MF}(1-\varepsilon)g(\rho_s - \rho_g) \text{ ----------2.5.1d}$$

Where
- ΔP = Pressure drop across the bed
- A_B = Cross-sectional area of the bed
- L_{mf} = Depth of bed at point of minimum fluidization
- ε_{mf} = Bed voidage at point of minimum fluidization
- ρ_g = Density of gas
- ρ_s = Density of solid
- g = acceleration due to gravity

Elutriation or maximum fluidization velocity (denoted U_t) is defined as the upper limit of gas velocities in a fluidized bed. In other words, it is the velocity at which a particle is entrained and carried away from the reactor in the gas stream and may be assumed to be the terminal falling velocity of the particles. The following expressions can be use to calculate the elutriation velocity depending on the Reynold number (N_{Rep}).

$$U_T = [d_p^2 g(\rho_s - \rho_g)]/18\mu \quad for\ N_{Re\,p} < 0.4 \text{ ----------2.5.1e}$$

$$U_T = 0.0178[g^2(\rho_s - \rho_g)^2 / \rho_s]^{1/3} d_p \quad 0.4 < N_{Rep} < 500 \text{ ----------2.5.1f}$$

$$U_T = [3.1 d_p g(\rho_s - \rho_g)/\rho_g]^{1/2} \text{ for } 500 < N_{Rep} < 2*10^5 \text{ ----------2.5.1g}$$

If we wish to minimise the amount of elutriation by the gas stream, the operating velocity U_O must lie between the minimum and maximum fluidisation velocities.

Different authors used various flow rates in their laboratory fluidized-bed chlorinators. Morris and Jensen, (1976) when chlorinating rutile, used a flow rate 10 times the minimum fluidizing velocity resulting in an equivalent linear gas velocity of 24cm/s, that is 6l/min at 25^{O}C through a 4.75cm inside diameter reactor tube. Sohn and Zhou, (1998) when chlorinating slag used a flow rate 10 times the minimum fluidizing velocity that resulted in a volumetric flowrate of 900cm^3/min at 25^{O}C in a 2.5cm inside diameter reactor tube. In the above cases, the average particle size was approximately the same, being 163μm and 177μm respectively.

2.5.2 Nature and Feedstock Requirements of the Chloride Process

The chloride process is a continuous one that operates in a fluidised-bed reactor. The raw material must have:

- Sufficient grain size and bulk density to minimize blow-over in the chlorination fluidized-bed reactor. In other words, most of the unreacted rutile and coke should not be carried over with the $TiCl_4$ (Minkler and Baroch, 1981). In this respect, natural rutile has an advantage over synthetic rutile, since the latter has a porous grain structure and lower bulk density (Stanaway, 1994).
- very low alkali earth metal content, especially MgO and CaO. Alkali earths form liquid chlorides at the chlorination temperatures. The liquid chlorides can defluidise and clog the reactor bed. In other words the liquid chlorides would block the pores of the fluidised bed thereby preventing free flow of the gas mixture, which may result in a large pressure drop in the lower part of the reactor. In addition, together with chromium, alkalis also act as fluxes promoting bed fusion (Stanaway, 1994). Also CaO reduces the chlorination of TiO_2 and SiO_2 by forming $CaO.TiO_2$ (Minkler and Baroch, 1981).

These effects are due to the fact that the chlorides of Mg and Ca have high boiling points (Minkler and Baroch, 1981) see table 2.5.2.

Table 2.5.2: Melting and Boiling Points of Chlorides of Calcium, Magnesium, Iron and Titanium, Sigma-Aldrich.

	$CaCl_2$	$MgCl_2$	$FeCl_3$	$TiCl_4$
Melting points (^{O}C)	782	714	306	-24.1
Boiling points (^{O}C)	1600	1412	316	136.4

- Low iron content to minimize the iron trichloride disposal problem, optimize plant capacity and minimize reagent consumption. $FeCl_3$ is a low boiling point impurity, which must be concentrated and removed in the purification stage by distilling out $TiCl_4$ or by centrifugation. High iron content in the ore will make it more difficult to concentrate and produce pure $TiCl_4$ gas (Stanaway, 1994 ; van Dyk et. al. 1999).
- Minimal chromium and vanadium, which impart potential toxicity to iron chloride waste (Stanaway, 1994 ; van Dyk et. al. 1999).
- Low silica, which could coat titanium minerals grains and so prevent their reaction with chlorine (Stanaway, 1994 ; van Dyk et. al. 1999). .
- Low tin and arsenic, which are difficult to separate in purification steps and which accumulate in the purified titanium tetrachloride (Stanaway, 1994 ; van Dyk et. al. 1999).
- Minimal uranium and thorium due to their undesirable radioactivity (Stanaway, 1994 ; van Dyk et. al. 1999).

2.5.3 Chlorination Kinetics of Titaniferous Feedstocks.

Rowe and Opie, (1955) reviewed the production and purification of titanium tetrachloride vapour. They used natural rutile feed (95% TiO_2) and chlorine in the presence of carbon at 700^{O}C in static-bed and fluidised-bed reactors. Briquettes of carbonised rutile-coke mixtures were fed at intervals to the stationary chlorination furnace, which was maintained at a temperature of 800^{O}C. Electrical energy supplied through carbon electrodes was used to supplement the heat produced during the reaction. Chlorine gas was introduced at a level slightly below the electrodes and as the chlorine rose through the furnace it reacted with the TiO_2-C briquettes. The gaseous product was led through the

dust catchers to a $TiCl_4$ condenser. The main disadvantages of the static-bed reactors are that they are discontinuous and they have to be periodically shut down to remove the residue or ashes that remained from the chlorination.

Modern plants make use of fluidised-bed reactors with closely sized solid feed materials (rutile, slag, ilmenite, and coke) to produce gaseous $TiCl_4$ (Rao and Chadwick, 1988; Stanaway, 1994; van Dyk et. al. 1999). In this type of reactor, the bed is usually supported on a perforated brick or ceramic plate. The titaniferous feedstock and coke are charged through a port above the bed (Rowe and Opie, 1955). The latter is kept in a fluidized state by the incoming reactive gas stream (Cl_2), which is admitted at high pressure. A small amount of N_2 is mixed with the input gas stream to regulate the temperature of the bed. Excellent heat transfer and high production rates make fluidised-bed reactors very attractive. The principal reactions in the chlorination of $TiO_{2(s)}$ are:

$$TiO_{2(s)} + 2C_{(s)} + 2Cl_{2(g)} \rightarrow TiCl_{4(g)} + 2CO_{(g)} \quad (T > 700^{O}C) \text{----------} 2.5.3a.$$

$$C_{(s)} + CO_{2(g)} \rightarrow 2CO_{(g)} \quad \text{(Boudouard reaction)} \text{----------} 2.5.3b.$$

$$TiO_{2(s)} + 2CO_{(g)} + 2Cl_{2(g)} \rightarrow TiCl_{4(g)} + 2CO_{2(g)} \text{----------} 2.5.3c.$$

For chlorination with a solid carbon reductant (equation 2.5.3a) above 700 ^{O}C CO is the dominant carbonaceous off-gas species.

Dunn, (1960) studied the chlorination rates of several titanium-containing materials in CO-Cl_2 gas mixture. He found that the chlorination rate of rutile depended linearly on the partial pressures of CO and chlorine in both fixed and fluidised–bed reactors. The rate expression relating the fraction of rutile chlorinated and the partial pressures of the two gases used is given as:

$$X = 55P_{CO}P_{Cl2}EXP[(-1.05 X10^{4})/T]t \text{----------} 2.5.3d$$

Where X = Fraction of rutile chlorinated
T = Temperature in Kelvin
P = partial pressures in atm
t = Time in minutes.

Bergholm, (1961) chlorinated Australian rutile in the presence of CO and carbon. For the CO-Cl_2 system, he found that the rate of reaction was proportional to the CO concentration but independent of Cl_2 concentration. The activation energies for these reactions are given in the table 2.5.3a below.

Table 2.5.3a: List of activation energies for the chlorination of titanium feedstock in different gas mixtures

Authors	Sample type	Reaction system	Activation energy (kJ/mol)	Temperature ranges (K)
Bergholm (1961)	Rutile	CO-Cl_2	104	
Dunn (1960)	Rutile & beneficiated ilmenite ("synthetic rutile")	CO-Cl_2	87.5	
Morris and Jensen (1976)	Rutile	CO-Cl_2	158	1143-1311
Morris and Jensen (1976)	Rutile	C - Cl_2	45.2	1143-1311
Sohn and Zhou (1999)	Rutile	CO-Cl_2	175	
Sohn and Zhou (1999)	beneficiated ilmenite ("synthetic rutile")	CO-Cl_2	156	
Jena et al (1998)	Pure TiO_2	C - Cl_2	130	773-873
Jena et al (1998)	Pure TiO_2	C - Cl_2	12	973-1273
Pistorius and le Roux (2002)	Titania slag	CO-Cl_2	28.8	1223
Sohn and Zhou (1998)	Titania slag	C - Cl_2	29	

Morris and Jensen, (1976) measured the porosity and density of Australian rutile particles at various degrees of chlorination. The results showed that Australian rutile was a non-porous solid, which undergoes no internal chlorination. Therefore, the reaction occurred exclusively at the surface of the particle at a rate proportional to the receding surface area. They developed an empirical equation based on the experimental results in both the $CO\text{-}Cl_2$ and $C\text{-}Cl_2$ systems respectively. The rate expressions they obtained are;

$(1-(1-X_B)^{1/3})/\theta = 6065(P_{CO}P_{Cl2})^{0.665}EXP(-37{,}800/RT)$----------2.5.3e

$$\left(1-(1-X_B)^{1/3}\right)/\theta = 0.294(P_{CO}^{0.692}d_C^{-0.55})(Coke/Ore)^{0.376}Exp\left(-10{,}820/RT\right)$$ --2.5.3f

Where k = rate constant

θ = Run time in minutes

d_c = Diameter of carbon particle (in cm)

P = Partial pressure (in atm(1.013×10^5 Pa))

X_B = fractional conversion

T = Reaction temperature (in K)

R = Universal gas constant (1.99 cal mol^{-1} K^{-1}).

The fractional order kinetics implied by the partial pressure exponents suggested that the TiO_2 surface was covered with relatively stable primary reaction products such as $TiCl_2$ and $TiOCl_2$, which limit the access of CO and Cl_2 to the surface, thereby reducing the apparent order of the reaction (Morris and Jensen, 1976). This could be attributed to the non-porous nature of rutile after the first few minutes of chlorination. Zhou et al. (1996) reported that further chlorination after the first 15 minutes leaves the rutile surface with some small grains, which are not properly oriented to react. It was also noted that natural rutile particles were more crystalline than synthetic rutile and thus undergo fewer microstructural changes during the chlorination reaction. Morris and Jensen, (1976) showed that, in the chlorination of Australian rutile, the activation energy for the $C\text{-}Cl_2$ system was very low compared to that of the $CO\text{-}Cl_2$ system with equal partial

pressure of chlorine. This result showed that, for rutile, coke was a more effective chlorination promoter than CO. At 1273K the rate with coke was nineteen times faster than that with CO as the reducing agent when chlorinating rutile. In the C-Cl_2 system, it was observed that the rate increases with increased coke/ore ratio (Morris and Jensen, 1976), equation 2.5.3f. However, for a fixed fluidised-bed volume, the amount of ore decreases correspondingly, so that there should exist an optimium coke/ore ratio for maximum efficiency of chlorine removal. The result of this study has been applied to minimize the chlorine losses in and preparing a comprehensive model of commercial fliudized-bed chlorinators (Morris and Jensen, 1976).

Recently, Jena et al. (1998) did a study on the kinetics of the carbothermic chlorination of fine TiO_2 powder (-32 to 25μm) by gaseous chlorine in a mixture with graphite powder (20-50 weight %) of the same particle size. The experiment was performed over two different temperature ranges, 773-873K and 973-1273K. They found that the fine powder of pure titanium dioxide mixed in a weight ratio of 3:2 with equally fine powdered pure graphite could be chlorinated appreciably (88%) in 75 minutes, even at the low temperature of 873K. They also found that unlike with CO, the amount of TiO_2 chlorinated increased with increase in the proportion of graphite up to 40 weight % after which the rate dropped. Chlorination, whether in the low (773-873K) or high (973-1273K) temperature ranges follows the topochemical reaction model as shown in equation 2.5.3g.

$$1-(1-\alpha)^{1/3} = Kt \text{----------} \quad 2.5.3g$$

Where α = fraction of TiO_2 reacted.
t = times in minutes
K = rate constant in min^{-1}

This indicated that the graphite must have taken part in the reaction directly (as the initial chlorination rate of TiO_2 was directly proportional to the initial amount of the graphite) and the decrease in the $\%TiO_2$ chlorinated at more than 40 weight

% graphite might be attributed to partial segregation between the particles because of the difference in their densities.

In all cases, the topochemical reaction model given in equation 2.5.3g provided a good fit to the amount of TiO_2 chlorinated (Jena et al., 1998). In the lower temperature range, the rate of chlorination was found to be proportional to P_{Cl2}, with activation energy of 130kJ/mol. The formation of the solid intermediate ($TiCl_2$) (reaction 2.5.3h), was suggested to be the rate-determining step in the lower temperature range (Jena et al. 1998). In the higher temperature range, the rate was proportional to the square root of P_{Cl2}, and reaction 2.5.3i was suggested to be the rate-determining step with activation energy as low as 12kJ/mol, since the production of $TiCl_2$ was considered to be fast. Experimental evidence for the formation of $TiCl_2$ had been provided by Zhou et al. (1996) who showed (using X-ray diffraction) that the final product on the surface layer was a solid solution of TiO and a small amount of Ti_3O_5.
Jena et al. (1998) suggested that the mechanism of the reaction was as follows:

$$TiO_{2(s)} + C_{(s)} + Cl_{2\,(g)} \rightarrow TiCl_{2(S)} + CO_{2\,(g)} \text{ ----------2.5.3h}$$

$$TiCl_{2(S)} + 1/2Cl_{2(g)} \rightarrow TiCl_{3(s)} \text{ ----------2.5.3i}$$

$$TiCl_{3(s)} + 1/2Cl_{2(g)} \rightarrow TiCl_{4\,(g)} \text{ ----------2.5.3j}$$

Finally, formation of the most stable gaseous phase, $TiCl_4$, according to reaction 2.5.3j, was considered to be fast under the reaction condition (Jena et al. 1998).
Rao and Chadwick (1988) studied the rate of chlorination of synthetic rutile in CO-Cl_2-He gas mixtures by thermogravimetry in the temperature range of 500-1000 ^{o}C. The synthetic rutile was prepared by oxidising a thin titanium metal foil. They found that the exponents for the partial pressures of CO and Cl_2 varied with the reaction temperature. They also found that phosgene ($COCl_2$) was formed when chlorine and carbon monoxide were mixed with each other under visible

light; this caused an anomaly in the experimental results below 800^{O}C. Above this temperature, phosgene decomposes and does not have any effect on the chlorination reaction.

Sohn and Zhou, (1999) showed that beneficiated ilmenite ("synthetic rutile") was a porous material. It is quite different from natural rutile, hence has a different chlorination rate. The sample used in their experiments was obtained by the Becher process (containing 92%TiO_2, 4%FeO, and 1% each of alumina, silica and magnesium oxide). During chlorination it was observed that the amount of titanium chlorinated at a given time increases with decreasing particle size, although the effect was not as large as that of natural rutile. The small dependence on superficial particle size was due to the presence of porosity. The shrinking core model was not applicable in this case, because the sample was porous and thus pore diffusion occurred simultaneously with chemical reaction inside the particle, which does not allow a topochemical reaction. The most appropriate rate expression was a pore-blocking rate law that gave the most satisfactory correlation of the results and is given as:

$K_{app}t = \lambda[\exp(x/\lambda)-1]$ ----------2.5.3k

Where x = fraction of TiO_2 converted

K_{app} = apparent rate constant

λ = constant independent of conversion

t = time in minutes

λ was related to the blockage, which inhibits access of reactant gases.

The origin of this relationship could be attributed to the numerous pores formed during beneficiation of the synthetic rutile (Sohn and Zhou, 1999). They also carried out experiments with various mixtures of carbon monoxide and chlorine gases to investigate the effect of partial pressures on the reaction rate at 900^{O}C. The particle size of the beneficiated ilmenite was 150-212μm. They found that the apparent rate constant, K_{app} , was a function of the partial pressure of the reactant gases and does not depend on particle size. They observed that the

rate of chlorination increases as the partial pressure of both CO and Cl_2 increases with chlorine giving a greater influence on the rate than CO. The rate expression in term of the Pco and P_{Cl2} is given as;

$$Kapp = KP_{CO}^{m} P_{Cl2}^{n} \text{ ---------- } 2.5.3l$$

Substituting equation 2.5.3l into equation 2.5.3k gives the overall rate expression for the reaction in terms of Pco and P_{Cl2}:

$$\lambda[\exp(x/\lambda)-1]-b = KP_{CO}^{0.82} P_{Cl2} t \text{ ---------- } 2.5.3m$$

Where b = $3.32d_p^{-0.8}$

d_p = particle size.

The rate of the chlorination reaction was also found to increase with temperature, and an apparent activation energy of 156kJ/mol was observed (Sohn and Zhou, 1999).

Zhou et al. (1996) investigated the effect of reaction time on the chlorination of ground titania slag particles with petroleum coke in a fluidized bed. The surfaces of the original slag particles contained no pores. When the samples were chlorinated at 1393K the % titanium and % iron chlorinated with time is given in the table 2.5.3b.

Table 2.5.3b: Effect of reaction time on the degree of chlorination of titania slag at 1393K[a].

Reaction time (min)	% titanium chlorinated	% iron chlorinated
15	11	70
30	28	80
90	95	99

a = Gas mixtures containing nitrogen, carbon monoxide and chlorine were used and the average particle size of the slag was 125μm.

At the end of the reaction time, SEM/EDX analysis showed that the surface was covered with small crystallites about 3μm in diameter. These crystallites were

composed mainly of rutile with small amounts of SiO_2, MgO, sometimes Al_2O_3, but no iron oxides. The chlorination reaction started with the easily chlorinated elements such as iron exposed on the surface leaving the particle surface with pores, crystallites of TiO_2 and other chlorination-resistant oxides. The outer shell was depleted of TiO_2 and gradually enriched with impurities that hinder the reaction by inhibiting the gas diffusion. This was confirmed by electron probe microanalysis (EPMA) of the particle cross-section which showed the elemental distribution where the unchlorinated impurities containing silica collected largely at the outer shell of the particle with the unreacted core consisting of TiO_2.

They also showed solid–state sintering and grain growth during the process at high temperature (1323K). At low temperature (1223K) the individual grains were very distinct while at intermediate temperature (1273K) a mixed microstructure was observed. It was apparent that, at lower temperature, the crystallites were larger than at higher temperatures. This may be partially due to the fact that lower temperature benefits the chlorination of iron relative to that of TiO_2 and partially due to the fact that, at lower temperatures, grain growth and sintering were slow. The significance of this is that a substantial amount of iron oxide contained in titania slag contributes significantly to the difference in the way the morphology of the solid changes during the chlorination reaction. When rutile is chlorinated, the generated surface morphology is largely limited to a narrow layer near the external surface. In the case of titania slag, the rapid chlorination of easily chlorinated iron oxide creates porosity that extends deeply into the interior of the particles. The remaining titanium oxide phase has a much greater surface area on which the chlorination reaction can occur. Thus, the rate of chlorination of titanium slag per unit area of the apparent external surface was expected to be considerably higher than that of rutile. The fact that a porous structure was established quickly by the chlorination of the easily chlorinated components was confirmed by the result of the B.E.T. specific surface area measurement. It showed that the surface area remained largely unchanged during the reaction after the rapid initial increase.

Sohn and Zhou, (1998) investigated the effect of temperature, chlorine partial pressure and the original slag size on chlorination rate (with coke as reductant). They found that, as the chlorine partial pressure increases, the rate of chlorination increases significantly with a reaction order of 1.5. The initial particle size of the slag was found to have a very limited effect on the rate of reaction. An increase in temperature was found to favour the rate of chlorination even though the effect was small with a very low activation energy of 29kJ/mol, table 2.5.3. Initially, the rate of reaction increased significantly, but as the reaction proceeded, this rate increase becomes less significant. This can be explained from the fact that the specific surface area of the slag increases tremendously after the first few seconds of the reaction, causing the rate of the reaction to increase. This can be attributed to the fact that, the slag becomes highly porous as the FeO in the slag is chlorinated (Zhou et al. 1996). The small induction time (t_o) at the beginning of the reaction, which mainly represents the time for the chlorination of the iron oxide and manganese oxide to create the porous titanium dioxide structure, increased with decreasing temperature (Sohn and Zhou, 1998). The relationship between the induction time and temperature is given as:

$t_o = 0.04\exp(6900/T)$ ----------2.5.3n

where t_o = induction time

t = time in minutes

T = Temperature in Kelvin

The chlorination rate of titania slag with petroleum coke in a fluidised-bed reactor can be summarized as:

$1-(1-X)^{1/3} = K_{app}(t-t_o)$, $t>t_o$ ----------2.5.3o

Le Roux, (2001) constructed a laboratory scale chlorinator which was used to compare the chlorination behaviour of block route slag to the literature data on rutile. The schematic diagram of the experimental set-up used is given in Fig 2.5.3a below.

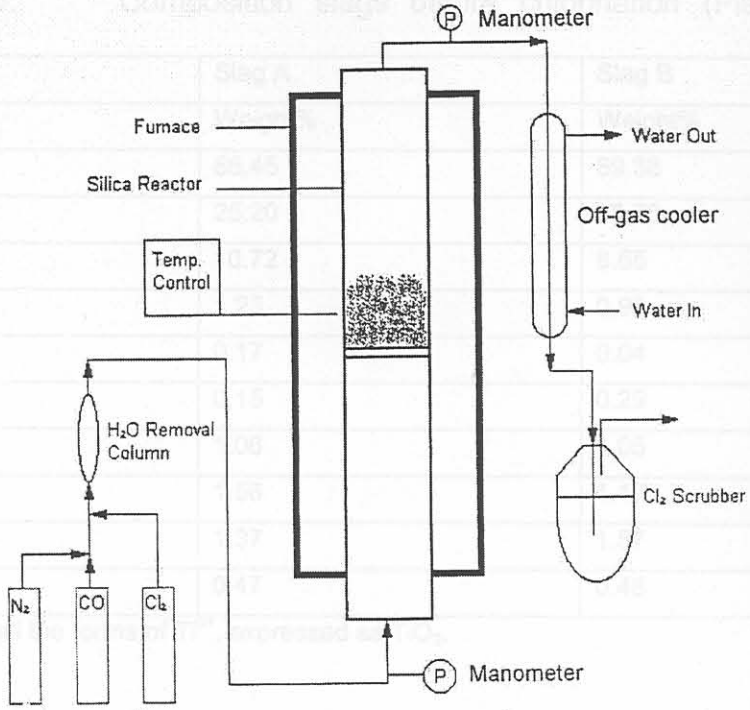

Fig 2.5.3a: Schematic Diagram of Laboratory Chlorinator (le Roux, 2001)

With the laboratory chlorinator, Pistorius and le Roux, (2002) determined the thermal, chemical and structural changes during initial chlorination of two block route slags whose compositions are given in table 2.5.3b.

Table 2.5.3b: Composition slags before chlorination (Pistorius and le Roux, 2002)

Compound	Slag A	Slag B
	Weight%	Weight%
TiO_2*	86.45	89.38
Tl_2O_3	25.20	33.70
FeO	10.72	8.65
Al_2O_3	1.23	0.93
Cr_2O_3	0.17	0.04
CaO	0.15	0.29
MgO	1.06	1.05
MnO	1.56	1.17
SiO_2	1.37	1.57
V_2O_5	0.47	0.48

TiO_2* denotes all the forms of Ti^{n+}, expressed as TiO_2.

The differences between these two slags are mainly in the Ti_2O_3 and FeO contents. In determining the effect of Ti^{3+} on chlorination of the slag they showed that Ti^{3+} (Ti_2O_3) in the slag acts as a reductant, and hence contributes to the chlorination of MnO and FeO present.

It was also shown that, in addition to its role as reductant, Ti_2O_3 was also chlorinated to $TiCl_4$, equation 2.5.3p

$$2CO + Ti_2O_3 + 4Cl_2 \rightarrow 2TiCl_4 + 3CO_2 \qquad \Delta H = -876.8 \text{ kJ/mol----------2.5.3p}$$

All these reactions were highly exothermic and the heat evolved could cause the fluidized bed to sinter and create hotspots in the bed. It was noticed that the bed temperature rose dramatically in the beginning of the experiments. This is illustrated in Fig 2.5.3b for the two slags.

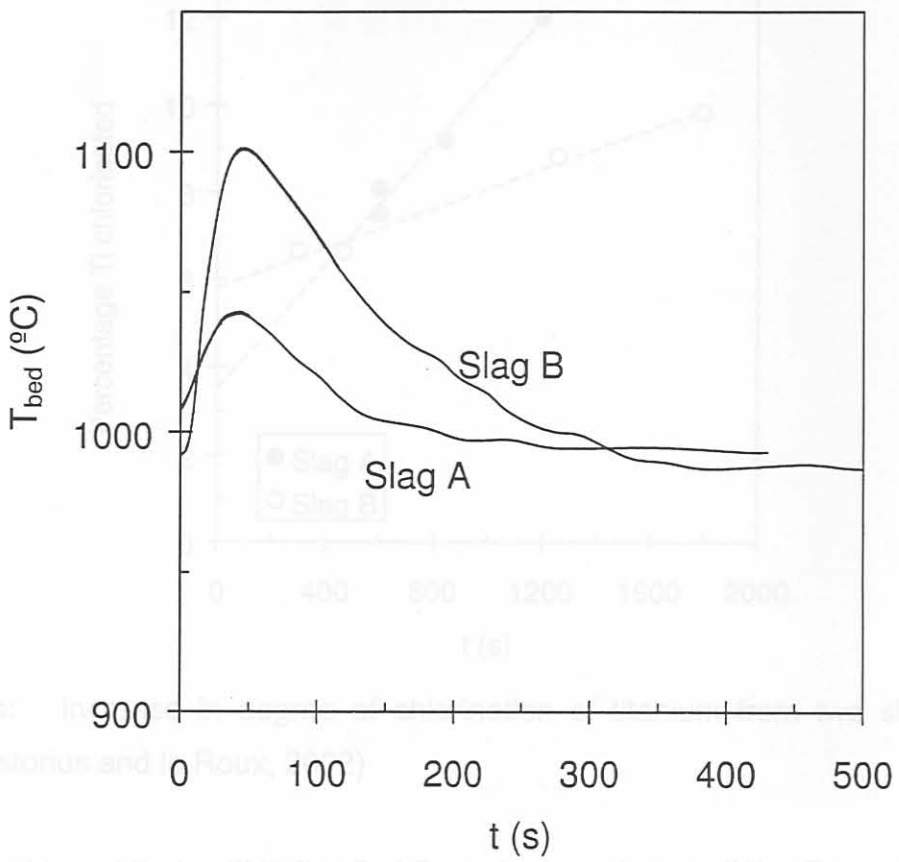

Figure 2.5.3b: Bed Temperature during Initial Chlorination of Slag A and B (Pistorius and le Roux, 2002).

It was shown that this rise was due to the presence of Ti_2O_3; the peak temperature depended on the amount of Ti_2O_3 present in the slag. Hence, a limited amount of Ti_2O_3 should be allowed in the slag.

They found that, the % of titanium chlorinated increases slowly with time (Fig 2.5.3c).

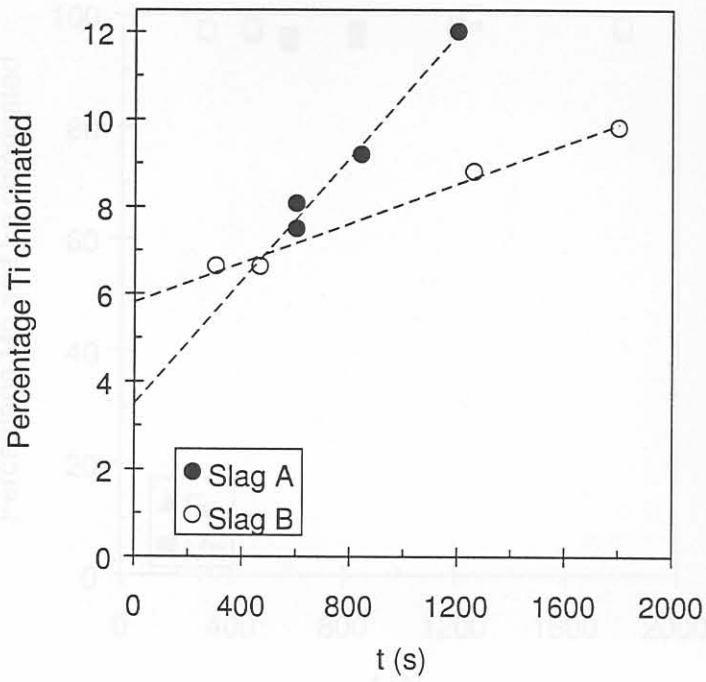

Fig 2.5.3c: Increase in degree of chlorination of titanium from two slags at 950°C (Pistorius and le Roux, 2002)

They also showed that, within the first five minutes, almost all the Fe and Mn in the slag were chlorinated (Fig. 2.5.3d). This was evident visually from the off-white appearance of the chlorinated slag, unlike the initial near-black particles. XRD analysis of the partially chlorinated samples showed the main crystalline phase to be rutile.

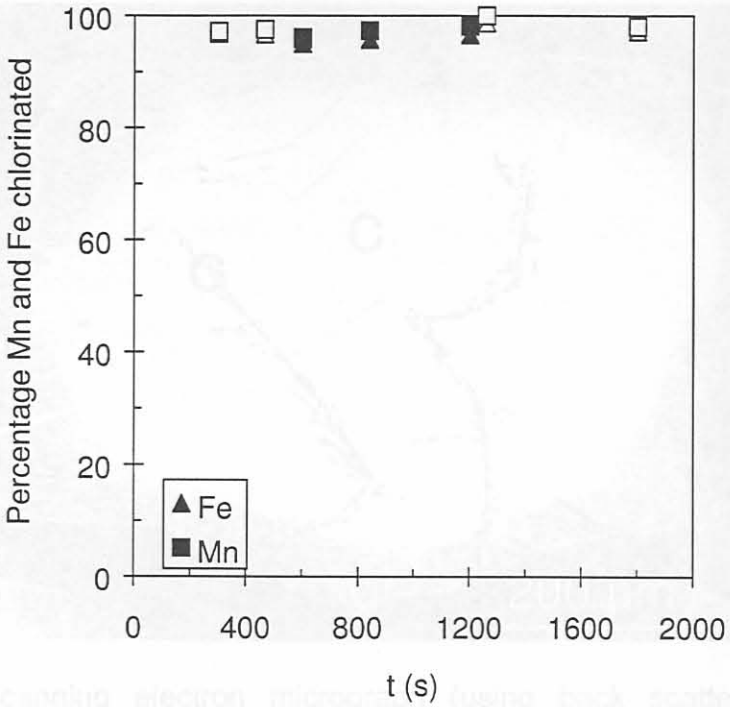

Fig 2.5.3d: Increase in the degree of chlorination of iron and manganese from slag A and B at 950 ^{O}C. Closed symbols are for slag A and open symbols for slag B, (Pistorius and le Roux, 2002).

The structural and compositional changes during the early chlorination of titania slag was also investigated. Results showed that a clear reaction front at the periphery of the particles was found during the first 30 seconds of chlorination. The front moves toward the particle centres at a rate of some 100μm/min. The chemical analyses showed that, ahead of the reaction front (towards the particle centre), the slag was unreacted whereas behind the reaction front it is essentially rutile (TiO_2), Fig 2.5.3e. The rutile matrix was highly porous due to the fast chlorination of oxides like FeO and MnO within the first few minutes of the process (Pistorius and le Roux, 2002). This agrees with the previous results, which showed that the chlorination of titania slag follows the topochemical reaction model (Zhou et al. 1996)

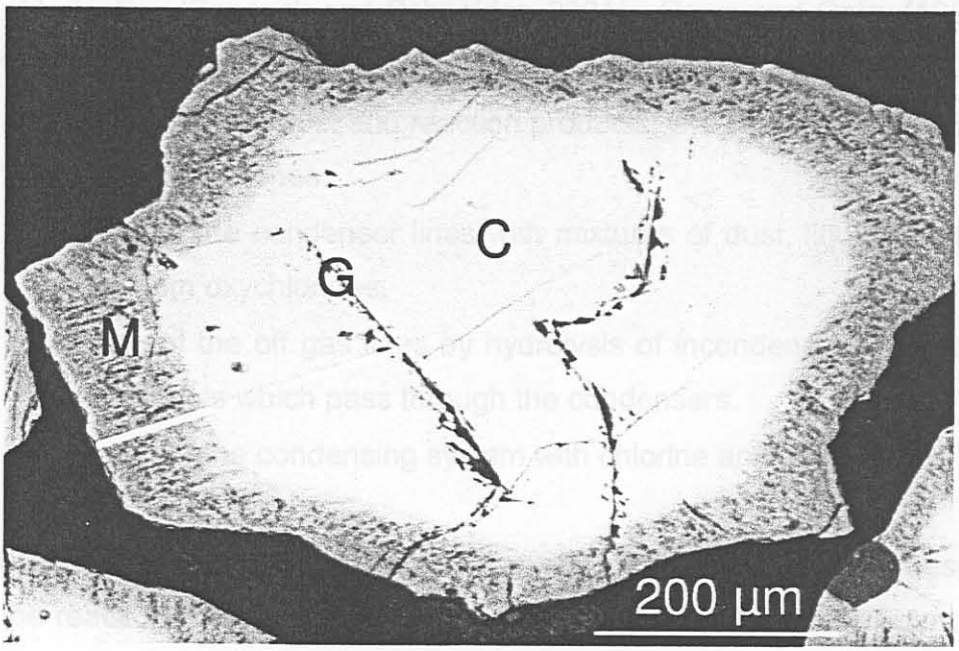

Fig 2.5.3e: Scanning electron micrograph (using back scattered electron imaging) of block route slag chlorinated for 30 seconds (Pistorius and le Roux, 2002).

2.6. Limitations of Fluidized-bed Technology and Possible Alternatives

Although fluidised-bed technology is used to produce titanium tetrachloride, there are strict feedstock requirements that limit the use of fluid-bed processing (Stanaway, 1994 ; van Dyk et al., 1999). Titanium ore feedstocks must fall within a narrow particle size range. Too-small particles will be elutriated from the fluidised-bed before sufficient residence time for the reaction, and too-large particles are difficult to fluidize. As stated before, the feedstock should contain very low amounts of alkaline earth metals, especially calcium oxide and to a lesser extent magnesium oxide. These chlorinate to form low vapour pressure or high boiling point liquid metal chlorides that tend to build up in the fluidised-bed. This could lead to defluidization, localised overheating and fusion of the bed. Also, the feedstock should contain low levels of chlorination inert components such as silica, which tend to accumulate in the bed and insulate the slag particles

from chlorination (Bonsack and Schneider, 2001). Rowe and Opie, (1955) also reported that the limitation of fluidised bed technology could be attributed to:

- Carry-over of fine dust and reaction products, which could only be partially removed by cyclones.
- Plugging of the condenser lines with mixtures of dust, liquid tetrachloride and titanium oxychlorides.
- Clogging of the off gas lines by hydrolysis of incondensable tetrachloride fogs and mists which pass through the condensers.
- Corrosion of the condensing system with chlorine and hydrochloric acid.

Rowe and Opie, (1955) showed that leakage of air into the system especially near the reaction zone could caused the oxidation of $FeCl_3$ and $TiCl_4$ to produce very fine Fe_2O_3 and TiO_2 particles, while moisture leakage will produce solid titanium oxychloride. Mechanical dust carry-over could be eliminated by careful charge preparation, close regulation of gas flows and adequate cyclone design (Rowe and Opie, 1955). They also mentioned that thorough drying of the charge and maintaining the system under a slight positive pressure could minimize these effects. Cooling of the exhausted gas mixture by refrigeration greatly reduced fog formation and minimized plugging in the system (Rowe and Opie, 1955).

Cole and Rowe, (1962) reported a flash chlorination technique capable of handling the unreacted fines. By charging the finely divided charge material of size between one and 50 microns into the bottom of the reactor bed chlorination occurs before the dust could pass through the bed.

Bonsack and Schneider, (2001) also showed that entrained-flow technology was a feasible alternative to the fluidised-bed process for producing titanium tetrachloride from feedstocks that are high in alkaline earth metals and chlorination inert components and that have a small particle size.

2.8. Conclusions

Despite the disadvantages of fluidised-bed technology, the method was used in this study for the chlorination of oxidised titania slag because of the following reasons. Firstly, the excellent heat transfer and high production rates make the reactor very attractive (Rao and Chadwick, 1988). Secondly, all chloride-route pigment producers use fluidised-bed chlorination reactors operating at 1000^{O}C or higher (Reeves and Reeves, 1997). Finally, the entrained-flow technology may be a feasible alternative but the method is new and has not yet been used by pigment producers (Bonsack and Scheider, 2001). However, one could recommend that more study be done on the entrained-flow method and how it can replace the fluidised-bed technique in the future.

3. MINERALOGY OF WATER - GRANULATED HIGH - TITANIA SLAG.

As mentioned earlier water granulated titania slag was produced in a pilot smelter by fragmenting and rapid quenching of the liquid slag with a jet of cold water. On the other hand, block route slag was produced by collecting the liquid slag in a ladle and allowing the slag to cool down slowly for several days or weeks depending on the size of the blocks (Bessinger et al. 2001).

3.1 Analytical Techniques Used:

The instruments and techniques used during the whole project include the following:

X-ray Diffraction (XRD):

This technique was used to identify the crystalline phases present in the slag samples. Quantitatively, it was used to estimate the amounts of each phase in the slag samples. The samples were micronized in a micronizing mill with corundum and transferred into the standard Siemens sample holders. The powder was then pressed into the holder using a glass slide ready for the analysis to be carried out. A Siemens D-501 instrument was used with a copper (CuKα(1.5418Å)) radiation source and the analyses were carried out at 25^{O}C. The step width (2θ) and collection time per step were 0.040^{O} and 1.5s respectively. Table 3.1 shows the peaks and the values of 2θ used to quantify the relative peak heights of the different phases.

Table 3.1: The values of 2θ used to identify various phases.

Phases	Angle (degree)
Rutile	27.46
Anatase	62.53
Ilmenite	62.41
M_3O_5	18.12

Scanning Electron Microscope (SEM):

The samples for SEM analysis were prepared by mounting the slag particles in an epoxy based material, polished to obtain a smooth surface and coated with carbon or gold for electronic conductivity. Backscattered (BS) electrons were used for generating backscatter electron images in which phases and morphology of the polished surfaces cross sections were distinguished. The higher the average atomic number, the more electrons were backscattered thus the brighter the image.

Energy Dispersive Spectrometry (EDS) was used for qualitative and quantitative analysis. The elements were identified from peak positions and the peak intensities were related to the concentrations. A standard least squares method of quantification was applied where each element had an ideal spectrum in the system unto which the elements in the samples were compared.

The typical acceleration voltage 20kV and working distance of about 22.5mm were used .

Electron Probe Microanalysis (EPMA):

This analytical tool was used for microanalysis. The wavelengths of the characteristic X-rays, together with comprehensive sets of standards, were used to quantify compositions. The acceleration voltage of 15kV and a working distance of 11mm were used. This enabled us to determine the different oxidation states of both iron and titanium in the slag.

Mössbauer Spectroscopic analysis:

^{57}Fe Mössbauer - effect spectroscopy (MES) is a (nuclear) γ - radiation resonance technique involving the recoil-free emission radiation by the source and subsequent recoil – free absorption of this radiation by ^{57}Fe nuclei in the sample. This is a non-destructive analytical tool for establishing the oxidation state of iron (e.g. ferrous or ferric) and quantifying the different phases within the slag samples. The spectra parameters that serve as fingerprints during the analysis include isomer shift δ, quadrupole splitting Δ and internal magnetic field

(B_{hf}) all of which serve to characterize the chemical state of Fe in the slag sample.

The slag samples were powdered and MES measurements were conducted at room temperature using a 5-10mCi 57Co (Rh) radioactive Mössbauer source. Typically, 40-50mg/cm^2 of sample was used which correspond to 5-10mg/cm^2 of Fe. This was considered to be optimal thickness to ensure acceptable (i.e. at least 30%) transmission of the incident radiation. This was also to have adequate quantities of the ^{57}Fe isotope in the sample to ensure a satisfactory signal to noise ratio after 12-25 hours accumulation periods. For samples which show low iron content data accumulation was extended for 3-4 days to obtain an adequate signal to noise ratio necessary for a reliable analysis. Data analysis was effected by using the non-linear least square Mössbauer analysing programme (NORMOS). Final parameters of the fitted components were compared with accepted literature values for various iron-oxides and iron-titanium oxides to make a phase identification. These measurements were carried out by staff of the Department of Physics at the University of the Witwatersrand.

X-ray Fluorescence analysis (XRF):

The chemical method of analysis provided information on the average or bulk composition of the slag samples. Like in XRD, the samples were powdered and the analyses were carried out. The results were used to determine the mass balance of the entire chlorination process.

3.2. Experimental

The water-granulated slag sample C, and block route slag of the campaign (BSC) were provided by Kumba resources for chlorination in a fluidised bed reactor. A typical block route slag (BRS) was also provided. The granulated slag and block route slag of the campaign (BSC) were produced from the same ilmenite source. The purpose of block route slags was to serve as a control to establish the effect of water granulation on the chlorination behaviour of the slag. The block route slag (BSC) was fragmented mechanically to a size range of 425-

600μm before chlorination. On the other hand, the granulated slag sample was supplied as a mixture of different size ranges. The as-received granulated samples were separated into different fractions by using laboratory sieves with the following sizes; 106μm, 425μm, 600μm, 1180μm, 1700μm, 2360μm, 3350μm, and 4750μm. Both particles of size ranges 425μm -600μm and 1700μm -2360μm of granulated slag sample C were used in the chlorination experiments. The granulated slag of size 1700-2360μm and the block route slag (BRS) were crushed and sieved to the required particle sizes ready for chlorination. Samples of all size ranges were powdered in a tungsten carbide mill for qualitative XRD analysis to be carried out. The powdered samples were further micronized for quantitative determination of the different phases present in the samples. Finally the as-received samples of all size ranges were mounted in an epoxy based material and polished for SEM analysis to be carried out.

3.3 Results

The size distribution of the granulated slag samples (C) is given in figure 3.3.1. The results show quite a wide size distribution, with most of the particles being larger than the top size of 850μm generally required by chlorinators. The particles of the granulated slag in the size range 1700-2360μm were irregular in shape, figure 4.3b while the particles in the size range 425-600μm were both cylindrical and spherical, figure 4.3c.

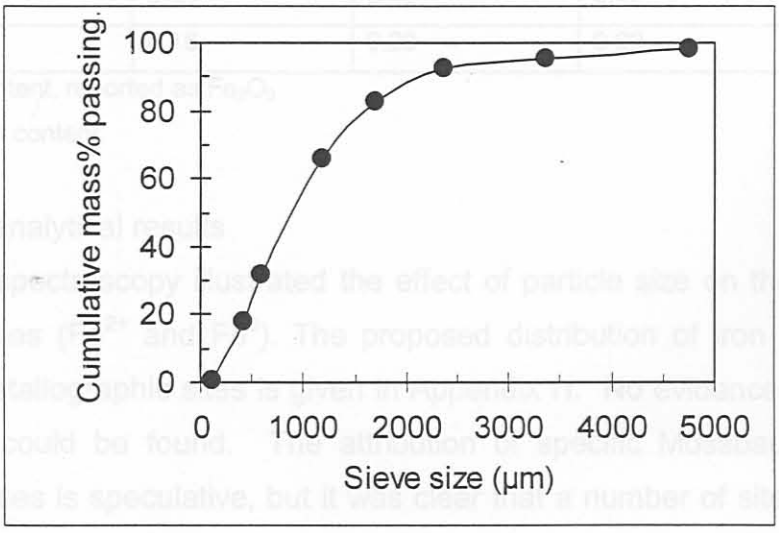

Figure 3.3.1: %Mass distribution of the particle sizes of granulated titania slag sample C.

X-Ray Floresence analytical results:

From the XRF analyses, the chemical composition of the block route slag (BRS) , block route slag of the campaign (BSC) and granulated slag samples C are given in table 3.2 below, which reflects a slightly high iron content in the block route slags as compared to the granulated slag. The detailed XRF analyses for the three sets of samples are given in appendix K.

Table 3.2: % chemical composition of the two sets of samples used during the chlorination experiments as determined by XRF analysis.

Oxides	BSC	BRS	Granulated slag sample C
Al_2O_3	0.98	0.74	0.75
CaO	0.08	0.19	0.20
Cr_2O_3	0.11	0.20	0.07
$Fe_2O_3(t)$[a]	13.62	16.99	11.22
MgO	1.02	1.47	1.06
MnO	1.53	1.13	1.21
SiO_2	1.04	1.21	1.28
$TiO_2(t)$[b]	85.13	81.37	85.04
V_2O_5	0.44	0.45	0.46
Zr_2O	0.18	0.20	0.22

a Total iron content, reported as Fe_2O_3

b Total titanium content.

Mössbauer analytical results

Mössbauer spectroscopy illustrated the effect of particle size on the distribution of iron species (Fe^{2+} and Fe^0). The proposed distribution of iron between the different crystallographic sites is given in Appendix H. No evidence of any ferric (Fe^{3+}) ions could be found. The attribution of specific Mössbauer peaks to specific phases is speculative, but it was clear that a number of sites in addition

to the ferrous pseudobrookite site were observed; these sites are variously labelled "ilmenite" and "sites A and B" in the Appendix H. However, these additional sites do indicate the presences of another iron-bearing phase in addition to the pseudobrookite. Solid solubility of a few percent of FeO in rutile has been reported, for the case where rutile formed by disproportionation of the M_3O_5 phase (oxidation of Ti^{3+} to Ti^{4+}, accompanied by reduction of FeO to Fe) (Teller et al. 1990). Hence it is suggested that at least some of the iron-filled sites detected by Mössbauer spectroscopy are in FeO-containing rutile.

XRD analytical results

The results generally showed that, four different phases, M_3O_5, rutile, anatase, and an ''iron titanium oxide'' were identified in the titania slags, figure 3.3.2. The relative amount of iron titanium oxide phase decreases as the particle size of the slag granules increases, appendix F. The ''iron titanium oxide'' phase is named as such in the XRD database; spectral information is available for this phase with the formula $Fe_{0.13}$ $Ti_{0.81}$ $O_{1.92}$ and shows a prominent peak at 2θ = 28.74. This is taken to be iron-containing rutile, which as mentioned above was also detected by MES.

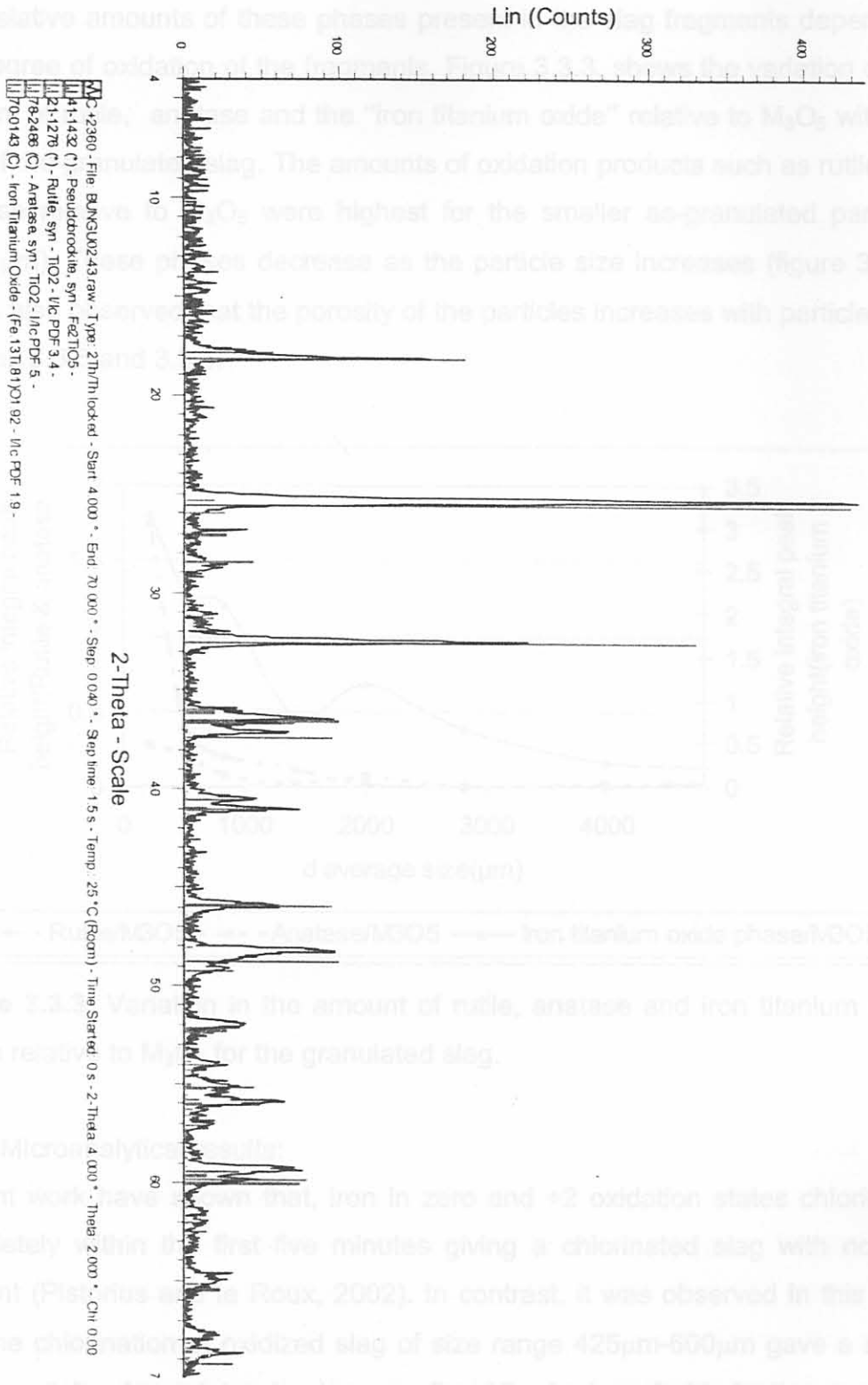

Figure 3.3.2: XRD spectrum showing four different phases present in oxidized titania slag of size range 2360 - 3350μm.

The relative amounts of these phases present in the slag fragments depend on the degree of oxidation of the fragments. Figure 3.3.3. shows the variation of the amount of rutile, anatase and the "iron titanium oxide" relative to M_3O_5 with the size of the granulated slag. The amounts of oxidation products such as rutile and anatase relative to M_3O_5 were highest for the smaller as-granulated particles (+106μm). These phases decrease as the particle size increases (figure 3.3.3). It was also observed that the porosity of the particles increases with particle size, Figures 3.3.5 and 3.3.6.

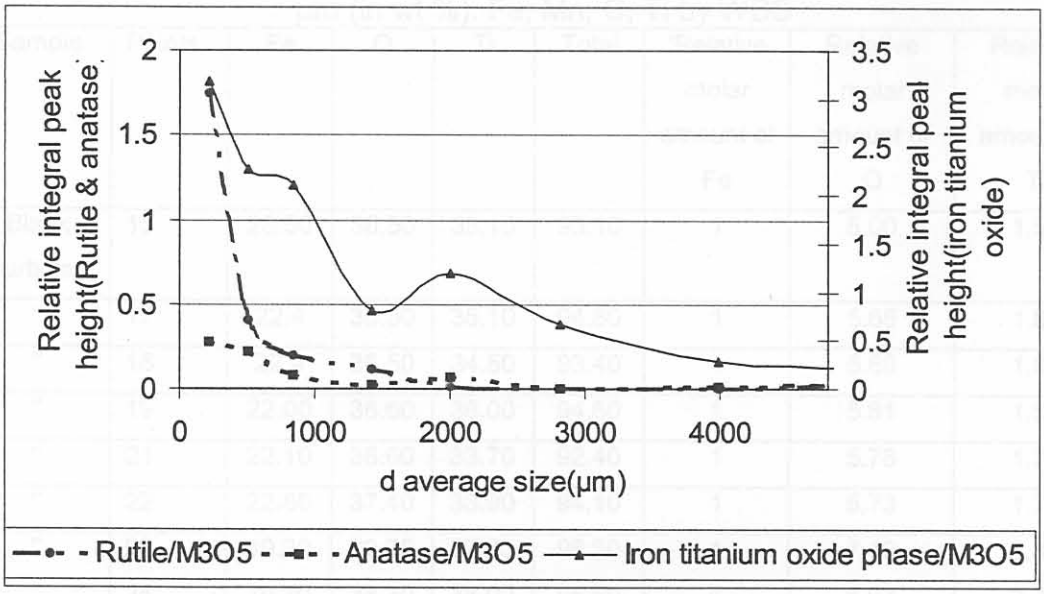

Figure 3.3.3: Variation in the amount of rutile, anatase and iron titanium oxide phase relative to M_3O_5 for the granulated slag.

WDS Microanalytical results:

Recent work have shown that, iron in zero and +2 oxidation states chlorinates completely within the first five minutes giving a chlorinated slag with no iron present (Pistorius and le Roux, 2002). In contrast, it was observed in this work that the chlorination of oxidized slag of size range 425μm-600μm gave a set of black particles (containing iron) even after 15 minutes of chlorination (as later shown in figure 4.4.3a and EDS analytical results, appendix E1). The off-white particles of the same size fractions and those of particles from the size range

1700μm-2360μm showed no iron present. The question was, in which oxidation state was the iron in these black particles? To provide answer to this question, the black particles were polished and sent for electron probe microanalysis where both WDS and EDS analysis were carried out.

Concentration in weight% of Fe, Mn, O, Ti and V were determined by WDS while the weight fraction of the other elements was determined by EDS. The full result is giving in appendix M while the result of the black particles is given in table 3.4

Table 3.4 Composition of chlorinated black particles of size range 425-600 μm (in wt %). Fe, Mn, O, Ti by WDS

Sample	Points	Fe	O	Ti	Total	'Relative molar amount of Fe	Relative molar amount of O	Relative molar amount of Ti
Black particles	15	25.50	36.50	33.10	95.10	1	5.00	1.52
"	17	22.4	36.30	36.10	94.80	1	5.66	1.88
"	18	22.4	36.50	34.50	93.40	1	5.69	1.80
"	19	22.00	36.60	36.00	94.60	1	5.81	1.91
"	21	22.10	36.60	33.70	92.40	1	5.78	1.78
"	22	22.80	37.40	33.90	94.10	1	5.73	1.74
"	23	19.20	39.20	37.80	96.20	1	7.13	2.30
"	24	19.30	38.30	38.00	95.60	1	6.93	2.30
"	25	25.20	40.30	34.70	100.20	1	5.58	1.61
Average						1	5.92	1.87

Results in table 3.4 show that Fe, O, Ti in the black particles occur in the approximate ratio of 1:6:2 giving the empirical formula as $FeTi_2O_6$. This cannot be the true formula, since charge balance and the large oxygen content would require titanium to be present in an oxidation state higher than Ti^{4+} and/or iron in an oxidation state higher than Fe^{3+}. However, it appears that the WDS method slightly over-analysed oxygen and it was concluded that iron and titanium were most likely present in their highest oxidation states in this phase. Finally it was concluded that, the chlorinated slag particles in the smaller size range appeared

black because they contain trivalent iron which could not be chlorinated, tetravalent titanium which chlorinates very slowly and magnesium oxide (See appendix M. The magnesium oxide chlorinates to form low vapour pressure or high boiling point liquid chlorides that tend to build up (Stanaway,1994).

SEM microanalysis.

Examination of the polished cross section slag samples using scanning electron microscope (SEM) with back-scattered electron imaging showed two main phases, appearing respectively higher-atomic number(Z) and lower-Z. Elemental analysis with energy dispersive spectroscopy (EDS) showed that the lower-Z regions were relatively titanium rich while the higher-Z regions were relatively iron rich, although with titanium remaining the main cation, see appendix A, B, C. Results for the smaller particles of size in the range 106-425μm, 425-600μm showed that oxidation had taken place throughout the particles, as the higher-Z and lower-Z regions were found randomly distributed throughout the particles. During this process, most of the Ti^{3+} in the M_3O_5 solid solution was converted to Ti^{4+} resulting in the precipitation of rutile and anatase as shown in the figure 3.3.4, hence confirming the previous results.

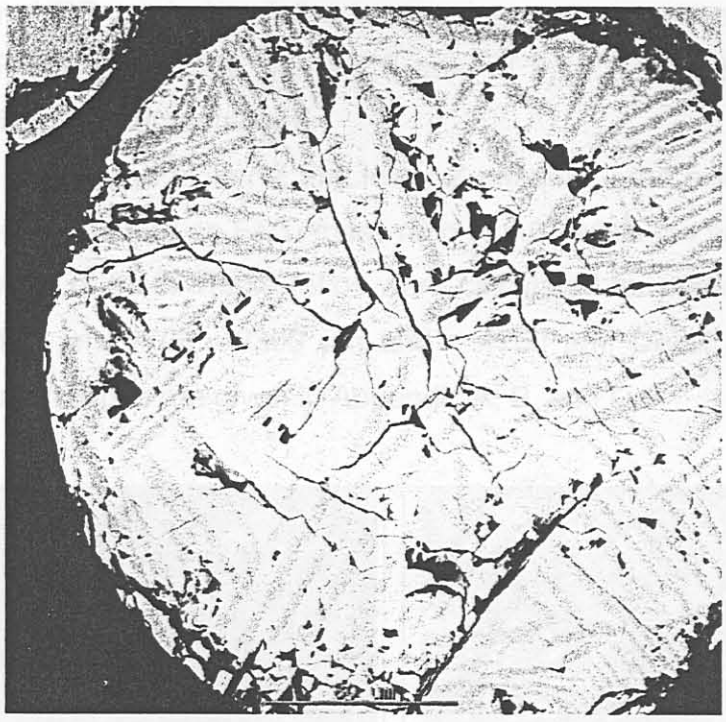

Fig 3.3.4; Granulated slag of size in the range 106-425μm showing random distribution of both lower-Z (iron-poor) and higher-Z (less iron-poor) phases throughout the particle. Back-scattered electron image.

Examination of the larger slag particles showed that, the relative extent (as a fraction of the total particle volume) of the oxidised (two-phased "higher-Z" and "lower-Z") regions decreases as the particle size of the granules increases, see for example figure 3.3.5a and b. These show the edge and centre part of the same particle in the size range of > 4750μm. The two-phased "higher-Z" and "lower-Z" regions are not randomly distributed throughout the particle but are more concentrated on the edge. This implied that the overall oxidation of the particles follows the topochemical reaction model. As stated earlier, the oxidized slags were found to be highly porous and the porosity increased with particle size. In contrast with this, the block route slag had a largely dense appearance, as can be seen in figure 3.3.6. The block route slag consisted primarily of M_3O_5 (pseudobrookite) phase. EDS analysis of uniform phase show an Fe/Ti ratio of 0.22 in addition to some impurities like Mg, Ca, Mn, and Al, see appendix D1.

Comparatively, XRF analysis of the same slag gave a percentage TiO_2 of 85.13% and Fe_2O_3 of 13.62% with Fe/Ti ratio of 0.16. These two results are comparable within experimental error.

EDS analysis of both the higher-Z and lower-Z phases of the oxidize slag show that the lower-Z phase had an Fe/Ti mass ratio of 0.03 while the higher-Z regions had an Fe/Ti ratio of 0.13. These ratios were calculated for particles in the size range 106 - 425 μm, 1700 - 2360 μm and > 4750 μm. Detail EDS analytical results for all size ranges are given in Appendix A, B, and C.

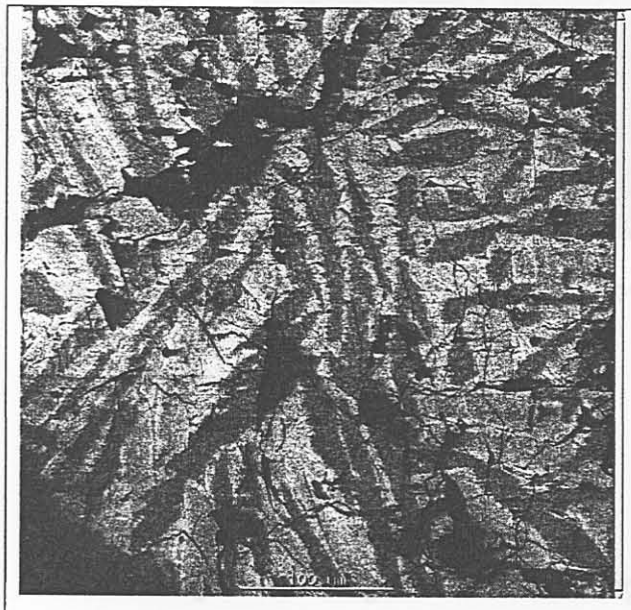

Fig. 3.3.5a; Edge of granulated slag of size range > 4750μm

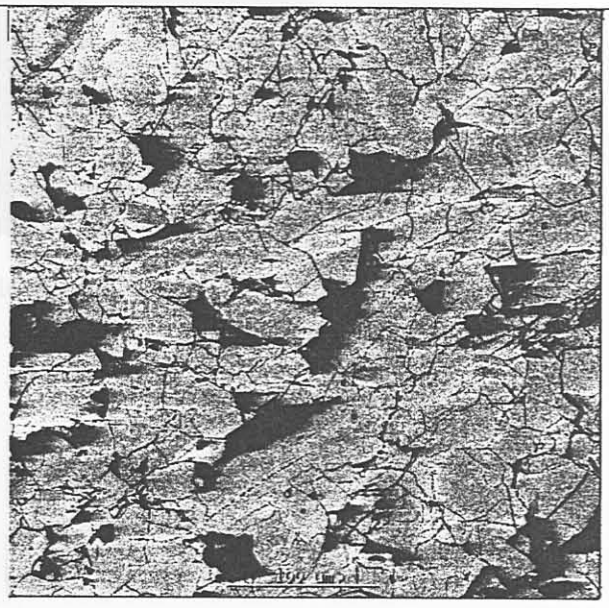

Fig. 3.3.5 b; Centre of granulated slag of size range > 4750μm

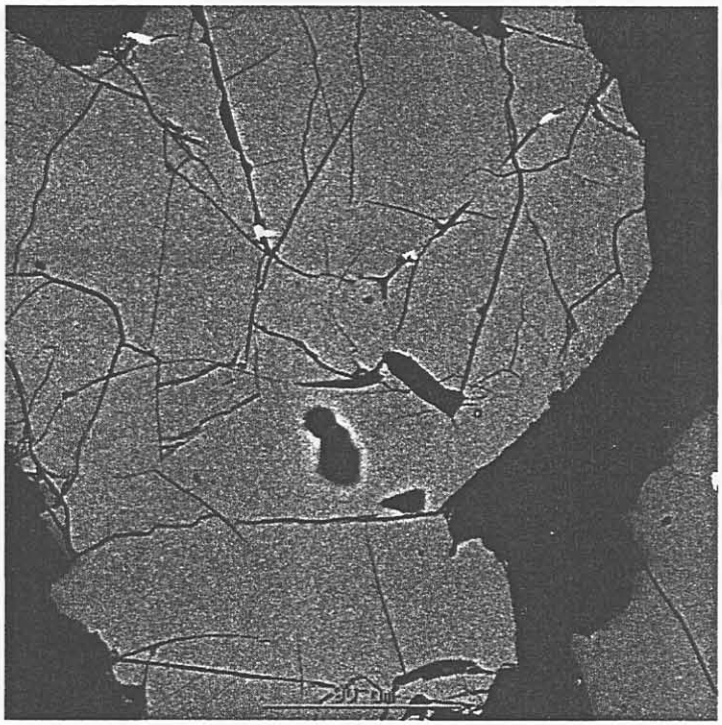

Fig. 3.3.6: SEM micrograph of block route slag of the campaign(BSC).

3.5 Conclusion:

Titania slag did undergo oxidation during water granulation, as a result, rutile (probably containing some FeO in solution for some particles) and iron-enriched pseudobrookite were formed as product phases. The nature of the black particles obtained after chlorination of the granulated slag in the size range 425-600μm showed that Fe^{2+} present in these particles did oxidise during granulation to Fe^{3+} as confirmed by WDS analysis. As mentioned earlier chlorination of this Fe^{3+} together with Ti^{4+} species in these particles is very slow, hence causing their non-porous nature. This might also be due to the presence of MgO which chlorinates to give high boiling point liquid. The association of the resultant chlorides and the slow reactive oxides account for the non-porosity of the slag. On the other hand, the second set of off–white particles obtained from the same batch of chlorinated sample and those of slag in the size range 1700-2360μm

showed that these sets of particles contain mostly iron in the +2 oxidation state. The rapid initial chlorination of this Fe^{2+} species to form gaseous $FeCl_3$ created porosity in the particles hence accounting for their off–white and porous nature. The oxidation of the granulated slag was much more complete for smaller particles, and a reaction front at the particle edge was found for larger particles. From this, it appears that controlling the size of the granulated particles is a feasible method to control the average degree of oxidation of the granulated product.

4: CHLORINATION OF HIGH TITANIA SLAG

4.1: Experimental

The chlorination of oxidised titania slag was carried out using a laboratory scale chlorinator as described before (le Roux, 2001). The schematic diagram is given in Fig.2.5.4a above. The chlorinator consists of a furnace within which a cylindrical silica reactor of 55mm external diameter was inserted. The reactor contained a silica perforated plate in the middle of the tube. A gas mixture of CO, Cl_2 and N_2 (whose flow rates were controlled by three rotameters) was passed through the bed from the bottom of the reactor. A mercury manometer was used to indicate the gauge pressure of the gas flowing into the reactor and a separate mercury manometer was also used to indicate the gauge pressure of the hot gas at the reactor exit. The hot gas mixture flowing out of the reactor was cooled through an off-gas condenser and finally through a scrubber system. The scrubber system consisted of four flasks. The first was empty and was used to collect the solid residues from the system. The second one contained tetrachloromethane which was used to absorbed titanium tetrachloride, while the two others contained concentrated sodium hydroxide which absorbed the excess chlorine from the product stream. Tetrachloromethane was used in the second container to avoid water which might react with titanium tetrachloride to form oxychloride which would block the pipes. The inner diameter of the off gas system through the condenser was in the range of 9mm. The flow rates at minimum and maximum fluidization velocities at room temperature were calculated to be 5.7 and 17.84l/mins respectively for particle sizes range 425μm-600μm. Detailed chlorination parameters are given in Appendix I.

4.2 Calibration of gas rotameters.

The three gas rotameters were calibrated to determine the relative amount of gases flowing through the reactor. The same procedure was used for nitrogen and carbon monoxide, and another for chlorine.

4.2.1: Nitrogen and carbon monoxide flowrates.

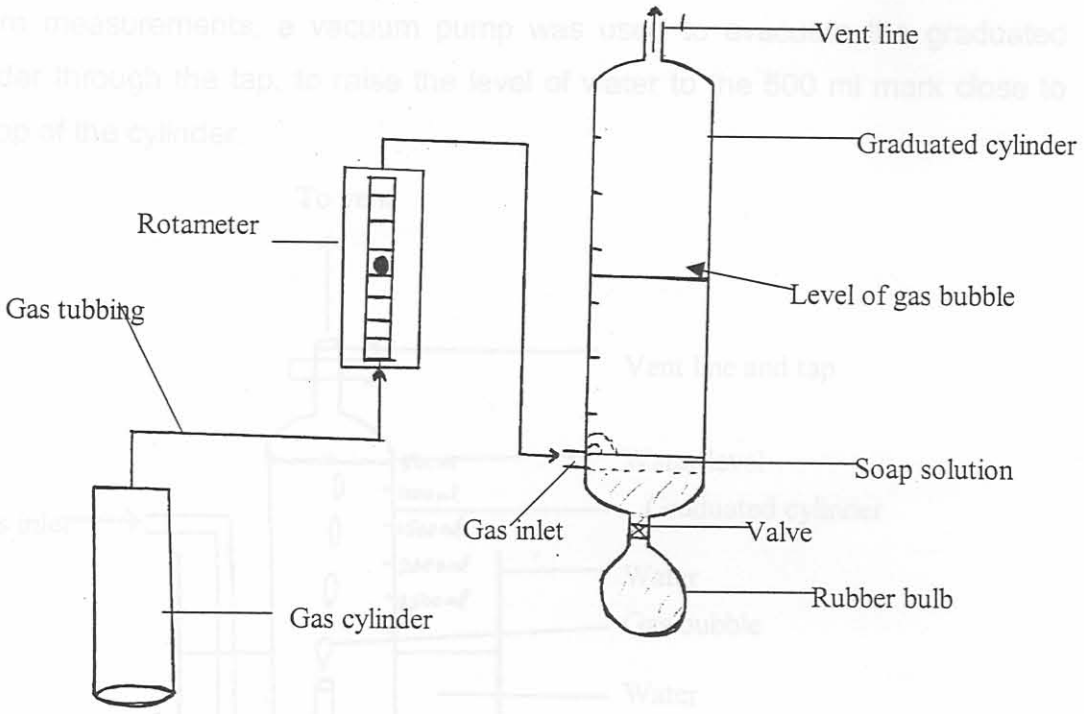

Figure 4.2.1: Schematic diagram of the apparatus used to determine the flowrate of CO and N_2.

The gases were allowed to flow from the regulator on the gas cylinder through the rotameters to a graduated cylinder containing liquid soap. The soap created bubbles which moved upward and exited through the vent line. The flowrates were measured by determining the time taken by the gas bubble to travel through a specific length of the cylinder. From the radius of the cylinder, the volume travelled by the gas during a specific time interval was determined and hence the

flow rate was calculated. The ambient temperature and atmospheric pressure of the laboratory were 22°C and 86kPa respectively.
The rubber bulb was used to increase the level of liquid soap in the cylinder when required.

Unfortunately, this method could not be used with chlorine since the gas reacted rapidly with the soap solution preventing the formation of the gas bubbles. The chlorine flowrate was determined by using the apparatus shown in figure 4.2.2 in which the gas flowing into an upturned graduated cylinder displaced water. Before measurements, a vacuum pump was used to evacuate the graduated cylinder through the tap, to raise the level of water to the 500 ml mark close to the top of the cylinder.

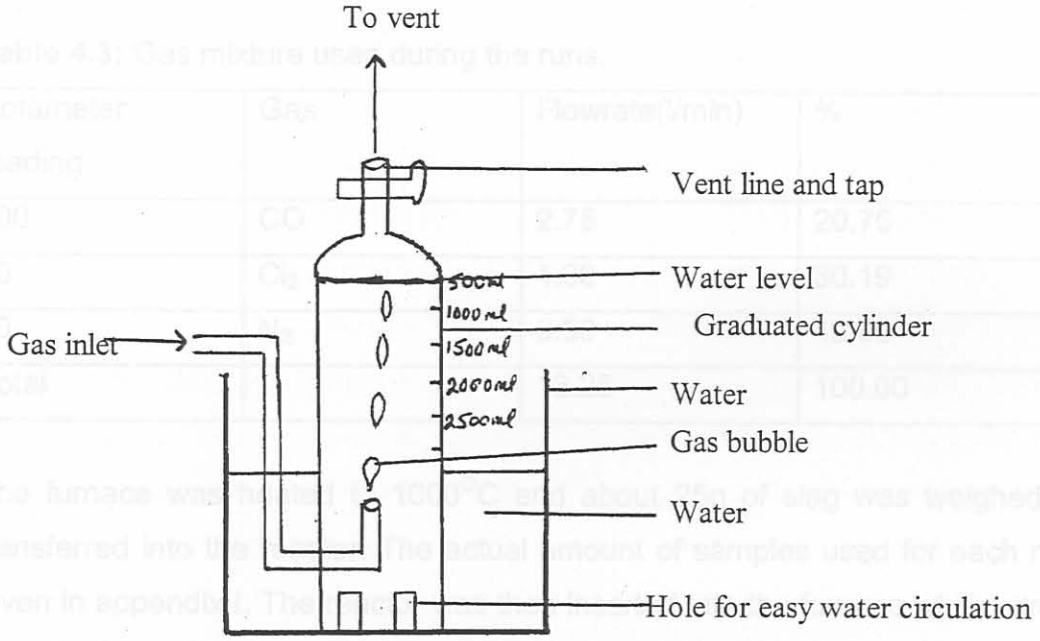

Figure 4.2.2: Schematic diagram of the apparatus used to determine the flowrate of chlorine.

After evacuation, the tap was closed and the tap exit connected to the vent line. The chlorine gas was allowed to flow through the rotameter into the graduated cylinder from below. As the chlorine flowed, the level of water fell; the time taken

for the level to fall from 500 to 1500 marks was recorded. The detailed result for the calibration of the three gases and the flowrate for each rotameter position are given in appendix J

4.3: Experimental Procedure

The following reaction parameters were used during all the runs.

Atmospheric pressure =86kPa

Total pressure that could be tolerated was in the range 108-115 kPa at a flowrate of 16.5l/min at 22.50^{O}C .

Reaction temperature = 1000 ^{O}C

The block route slags and granulated slag of size range 1700-2360μm were fragmented to the reaction particle size range of 425μm-600μm.

Table 4.3: Gas mixture used during the runs.

Rotameter reading	Gas	Flowrate(l/min)	%
100	CO	2.75	20.75
20	Cl_2	4.00	30.19
30	N_2	6.50	49.06
Total		13.25	100.00

The furnace was heated to 1000^{O}C and about 25g of slag was weighed and transferred into the reactor. The actual amount of samples used for each run is given in appendix I. The reactor was then inserted into the furnace while nitrogen was flowing through at a flow rate of 6.5l/min, which was above the minimum fluidization velocity. When the whole system was gas tight and the temperature at 1000^{O}C, CO and chlorine at flow rates of 2.75 and 4.0l/min respectively were mixed and flowed through the system with the nitrogen. Simultaneously, the stopwatch was started and the time taken for the reaction was recorded. The reaction was repeated for 5, 10, and 15 minutes respectively. At the end of each reaction time, CO and chlorine flows were stopped while nitrogen was allowed to

continue flowing at the same rate to flush the system for at least 5 minutes. The reactor was then disconnected, removed from the furnace and allowed to cool down. The mass of the product was determined (see Appendix I) and samples were collected for SEM, XRD, EDS, WDS and XRF analysis. The temperature rise of the fluidized bed during the first few minutes of chlorination was recorded using a K-type thermocouple. The tips of both the internal and external thermocouples were placed at the centre part of the furnace where the bed is expected to fluidize and the temperature was at 1000^{O}C. The thermocouple within the reactor was enclosed in a silica sheath. The room temperature for each run was also recorded (see Appendix I).

4.3.1: Problems encountered during the chlorination process.

The chlorination reaction proceeded with a lot of difficulties due to blocking of the pipes before and after the sodium hydroxide scrubbers. The pipes before the scrubber were blocked with a mixture of manganese (II), titanium (IV) and iron (III) chlorides. According to (le Roux, 2001), the blocking of the pipes after the NaOH scrubber was due to the formation of $Ti(OH)_4$. These blockages resulted in high back pressure within the system, which tended to force the mercury from the manometers. These blockages were observed to be more pronounced with the block route slag and granulated slag of size range 1700-2360μm than with smaller sizes. In other words, for the granulated slag of original size range 425μm-600μm, the chlorination proceeded smoothly without any problems. The blockage was due to the higher chlorination rates of the first two slags, unlike the slag of smaller sizes (where especially iron oxide was only partially eliminated during initial chlorination). It was also found that the small diameter (9mm) of the off-gas system contributed to the blockage. Redesigning the off-gas system to increase the inner diameter to 14.4mm minimized this problem. The part of the system whose inner diameter could not be increased was washed after each run to minimize blockage. This was done by removing these parts, washing with water then with acetone, drying before assembling for the next run. Replacing the solution in the second scrubber with carbon tetrachloride also prevented the

blockage of the pipe. When all these adjustments were made, the absolute pressure in the system for all the runs was reduced to the range 87.1-96.9 kPa. Finally, white foams were also observed during the runs due to the reaction between sodium hydroxide and chlorine as in equation 4.3.

$$NaOH + Cl_2 \rightarrow NaOCl + HCl \quad \text{---------- 4.3}$$

Foaming appeared to occur when the NaOH solution was saturated with chlorine. The foam also blocked the pipes creating high back pressure in the system.

4.3.2 Optical microscopic examination of the unchlorinated slags.

Optically (under a stereo microscope) the unchlorinated slags appeared black and the intensity of the colour was highest with the unoxidized block route slags as compared to the oxidized slags. The particles of the block route slag and granulated slag of larger sizes (which was crushed before chlorination) were found to be irregular while those of the granulated slag of smaller sizes were more spherical and cylindrical. See Figures 4.3 a, b, and c.

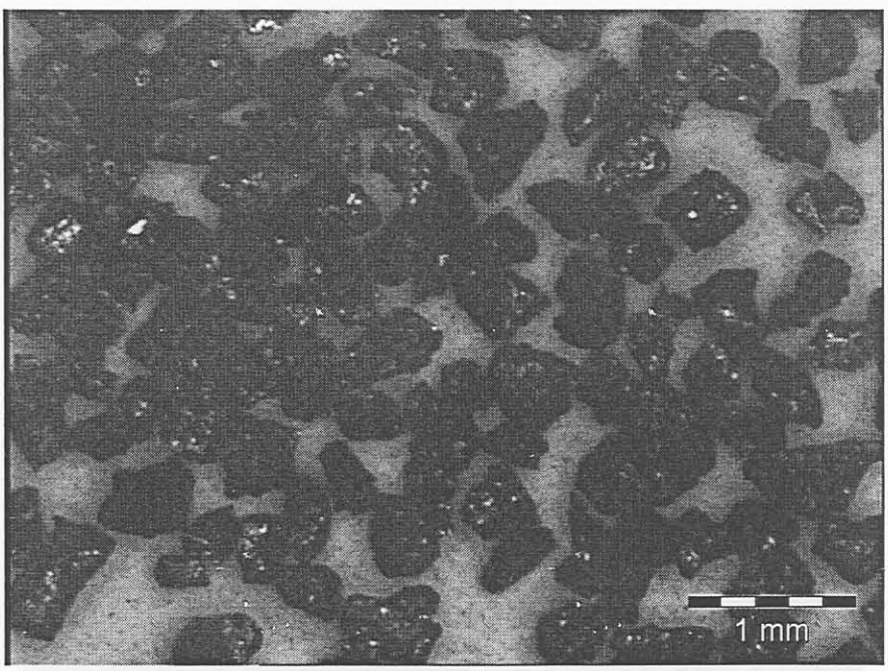

Figure 4.3 a: Optical micrograph of unchlorinated block route slag of the campaign (BSC).

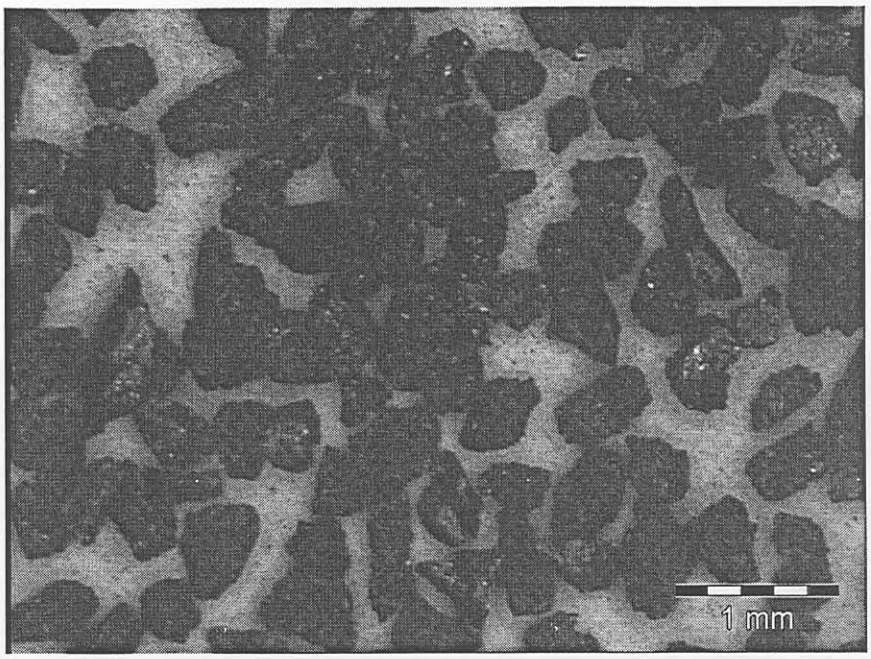

Figure 4.3 b: Optical micrograph of granulated slag of size range 1700μm-2360μm after crushing to the size range 425-600μm, and before chlorination.

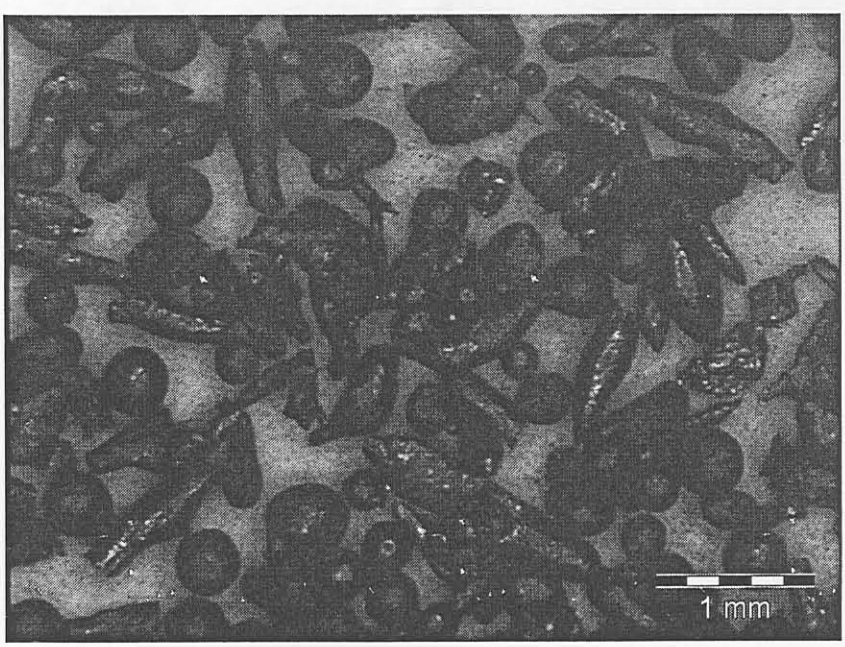

Figure 4.3 c: Optical micrograph of granulated slag of size range 425μm-600μm.

4.4 Results and Discussion.

4.4.1 Optical microscopic analysis of chlorinated slags.

When the block route slag of the campaign (BSC) and granulated slag of size 1700-2360μm were chlorinated for 5, 10, and 15 minutes, the product obtained consisted of off-white particles. Optical images of particles chlorinated for 15 minutes are shown in figure 4.4.1 a, and b.

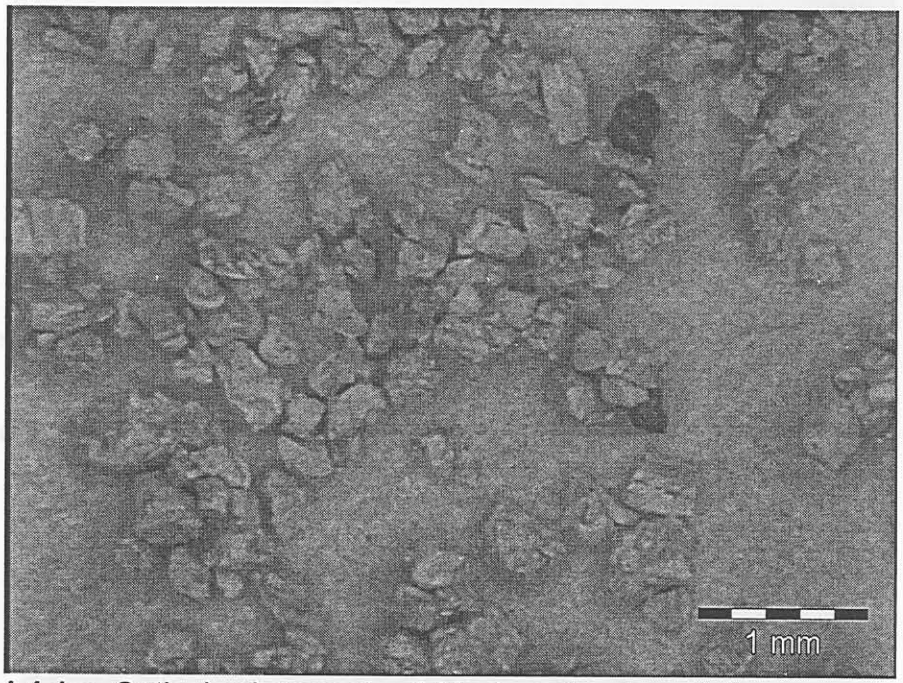

Figure 4.4.1a: Optical micrograph of block route slag of the campaign (BSC) chlorinated for 15 minutes.

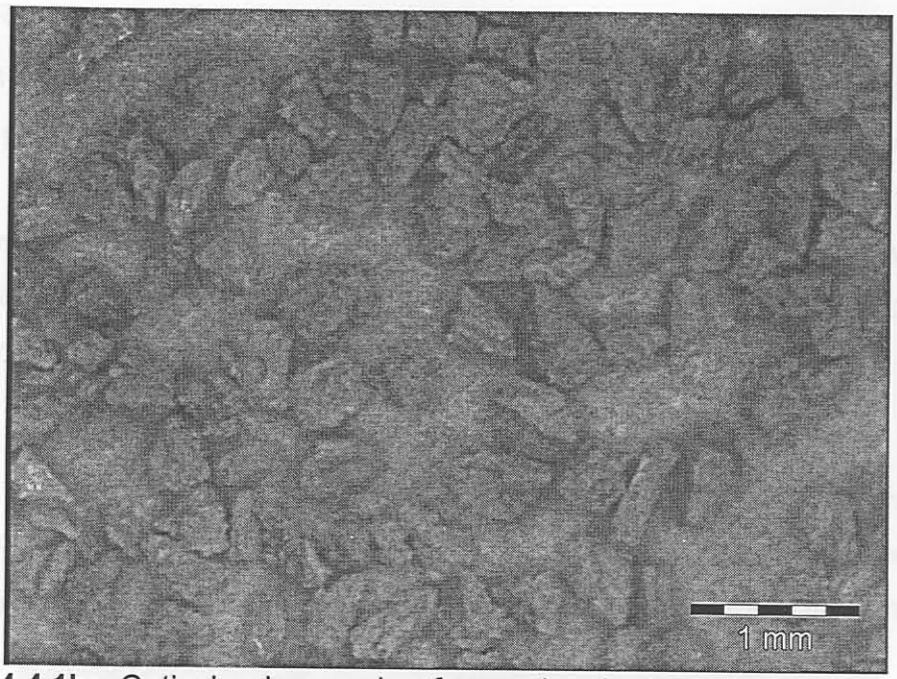

Figure 4.4.1b: Optical micrograph of granulated slag of size range 1700-2360μm, chlorinated for 15 minutes.

On the other hand, chlorination of the slag of size range 425μm-600μm gave a mixture of black and off-white particles, figure 4.4.1 c.

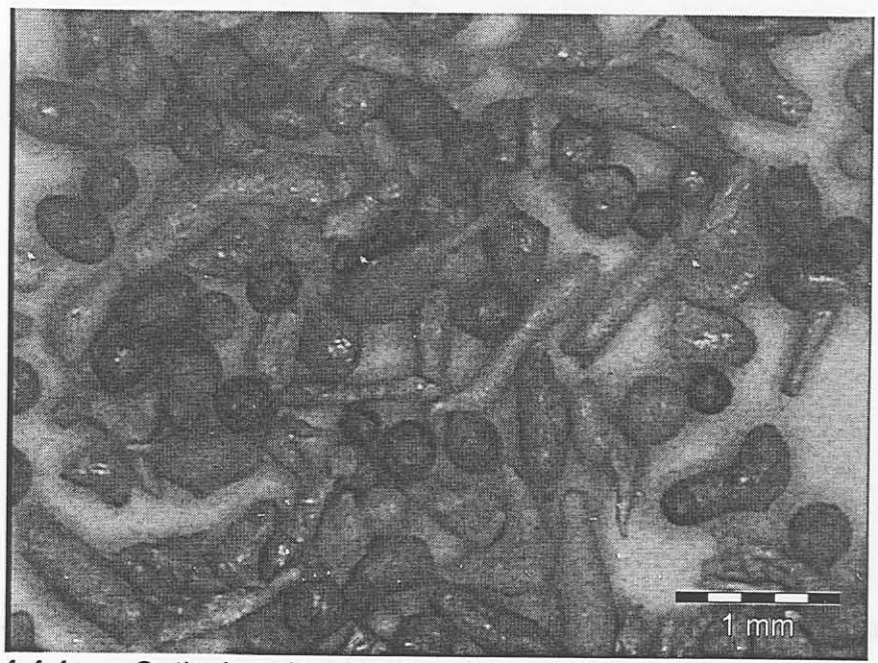

Figure 4.4.1c: Optical micrograph of granulated slag of size range 425μm-600μm, chlorinated for 15 minutes.

4.4.2 XRD Analytical Results.

Analysis of the three sets of samples chlorinated for 5,10 and 15 minutes showed that the products contained a major phase, rutile, with relatively small amounts of ilmenite and pseudobrookite, Appendix G. This result agrees with the XRF results which showed that almost all the MnO and FeO are removed within the first 5 minutes of chlorination, Appendix K. As these impurities were removed, the rutile content increases with chlorination time, Figure 4.6.3 below.

4.4.3: SEM Analytical Result.

The two types of particles obtained after chlorination of the smaller granulated particles ("black and off-white", as shown in figure 4.4.1c) were separated manually, polished and examined by SEM with backscattered electron imaging.

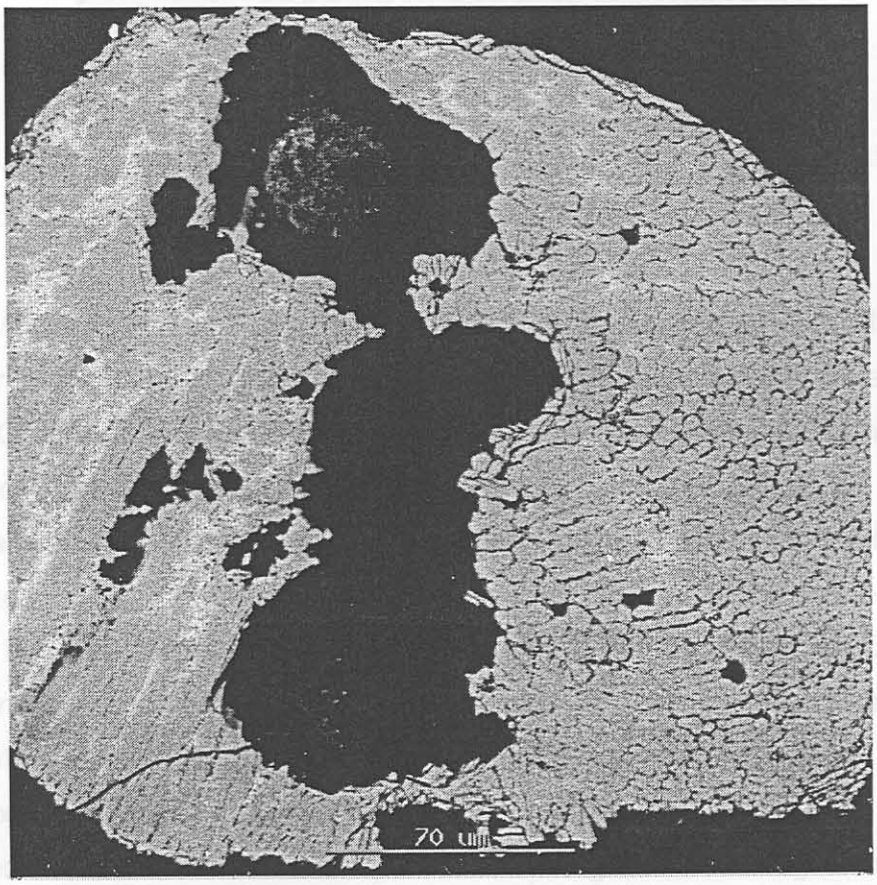

Figure 4.4.3a: SEM micrograph of a black particle of slag of size range 425-600μm chlorinated for 15 minutes .

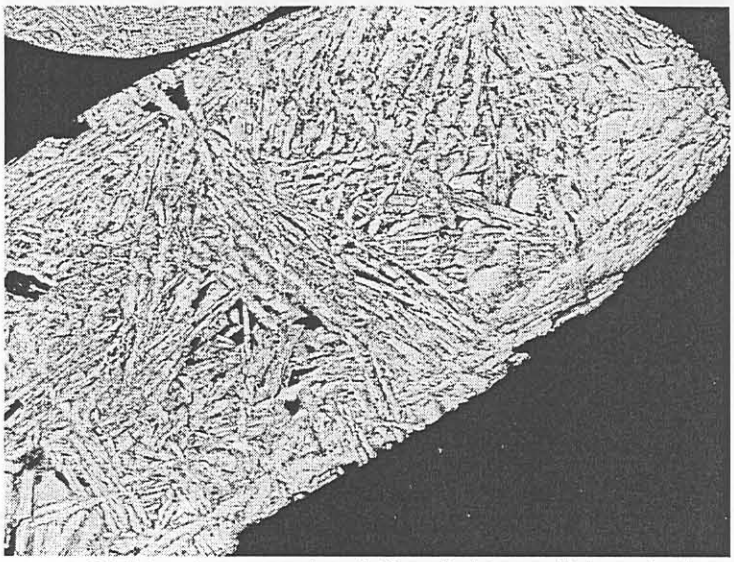

Figure 4.4.3b: SEM micrograph of the light particle of slag of size range 425-600μm chlorinated for 15 minutes

The SEM micrographs showed that the black particles were smooth, dense with large pores and contain light and dark regions similar to the original slag (Figure 4.4.3a). On the other hand the light particles show a uniformly porous phase with needles of rutile (Fig 4.4.3b).

EDS analysis show that the higher-Z regions of the black particles chlorinated for 15 minutes contained an average of Fe/Ti ratio of 0.37 while the lower-Z regions of these black particles contained an average ratio of 0.04, Appendix E1. On the other hand, the edge and central portions of the light particles also chlorinated for 15 minutes showed a very low content of Fe with an Fe/Ti ratio of 0.007, Appendix E2.

As stated earlier, the chlorinated product of the granulated slag of size range 1700μm-2360μm consisted of uniformly off-white particles similar to the light particles above, Figure 4.4.3c.

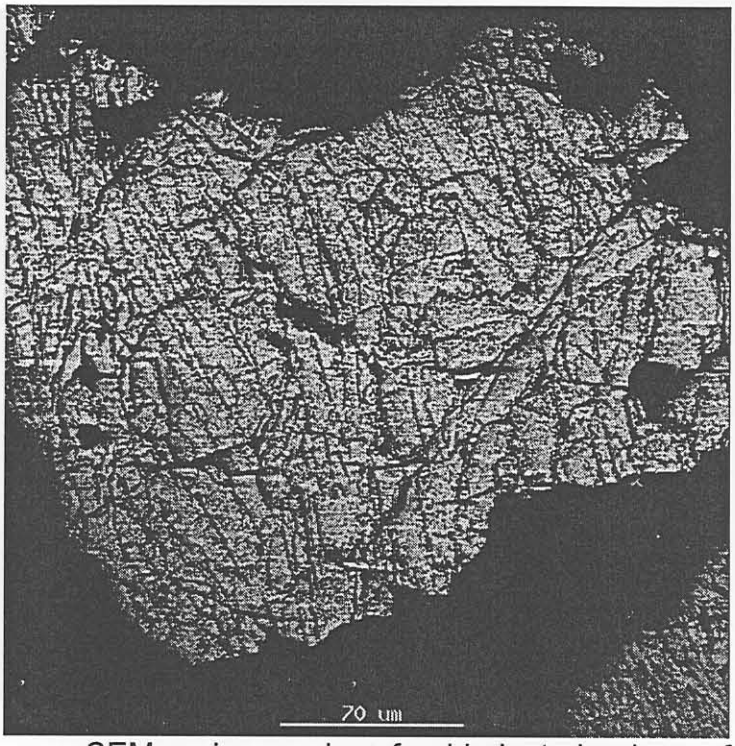

Figure 4.4.3c: SEM micrograph of chlorinated slag of size range 1700μm-2360μm chlorinated for 15 minutes.

These results (Figure 4.4.3c) show that, these particles were highly porous and the total porosity was higher than in the case of the slag of size range 425μm-600μm, Fig 4.4.3a .

The rutile needles were also observed and EDS analysis confirms that the particles had a very low content of Fe, Appendix E3

Chlorination of block route slag for 5, 10 and 15 minutes also gave uniformly off-white particles, figure 4.4.1a. The chlorinated product was polished and studied using SEM. Results show that the samples chlorinated for 5 minutes consisted of both higher-Z and lower-Z regions. The higher-Z regions were very small and were found close to the centre of the particles while the lower-Z regions of the particles appeared dark, figure 4.4.3d. The higher-Z region were iron-rich and appeared to be unchlorinated M_3O_5, while the lower-Z outer regions were mainly rutile.

Figure 4.4.3d: SEM micrograph of chlorinated block route slag of the Campaign(BSC) chlorinated for 5 minutes.

EDS analysis of the higher-Z regions show a relatively high Fe/Ti ratio of 0.06 while analysis of the edge gave a very low Fe/Ti ratio of 0.001, Appendix E4.

Generally, the block route slags and granulated slag of size range 1700μm-2360μm were more easily chlorinated than those in the size range 425μm-600μm. This was because the former contained oxides of Fe(II) and Mn(II) that were almost completely chlorinated within the first few minutes of chlorination thereby creating porosity in the particles (see also figures 4.6.1 a and b). This porosity provided a large surface area thereby increasing the chlorination rate for these sets of particles. The slag of size range 425μm-600μm consisted of two types of particles. One type contained iron in the +2 oxidation state which chlorinated easily to give the porous off-white particles after the first few minutes of the process. The second type was non-porous due to the presence of iron in the +3 and titanium in the +4 oxidation states which were difficult to chlorinate. These particles remained black (indicative of significant iron) even after 15 minutes of chlorination. The fact that only part of the iron

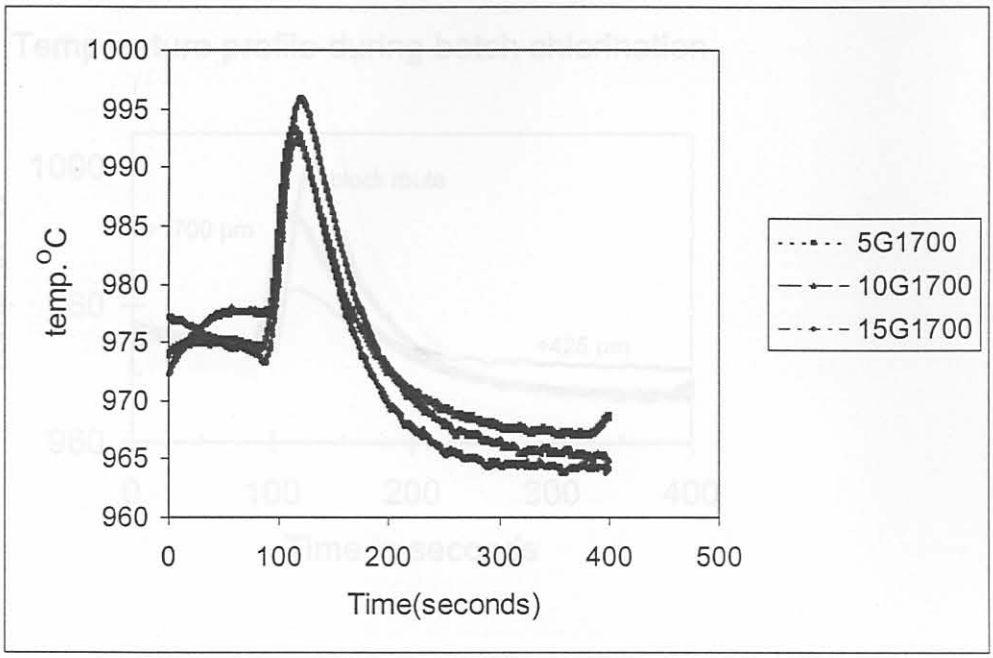

Figure 4.5a Temperature profile during initial chlorination of slag of size range 1700 - 2360μm, (results from three repeat runs shown).

Pistorius and le Roux, (2002) showed that this temperature increase during chlorination was related directly to the amount of Ti_2O_3 present in the slag. The differences in the temperature changes for the three slag samples shown in figure 4.5b could hence be taken to be related to the levels of FeO, Ti_2O_3 and impurity oxides in the slag. The temperature increased by 30°C for block route slag (BSC), 20°C for slag of size range 1700 - 2360μm and 8°C for slag of size range 425 - 600μm reflecting their different Ti_2O_3 contents. During water granulation of the slag, some of the Fe^{2+} and Ti^{3+} were converted to Fe^{3+} and Ti^{4+} respectively. Thus, the amount of Ti^{3+} in the slag decreases in the order 425-600μm < 1700-2360μm < BSC; this explains why the heat evolved during initial chlorination decreases in the same order.

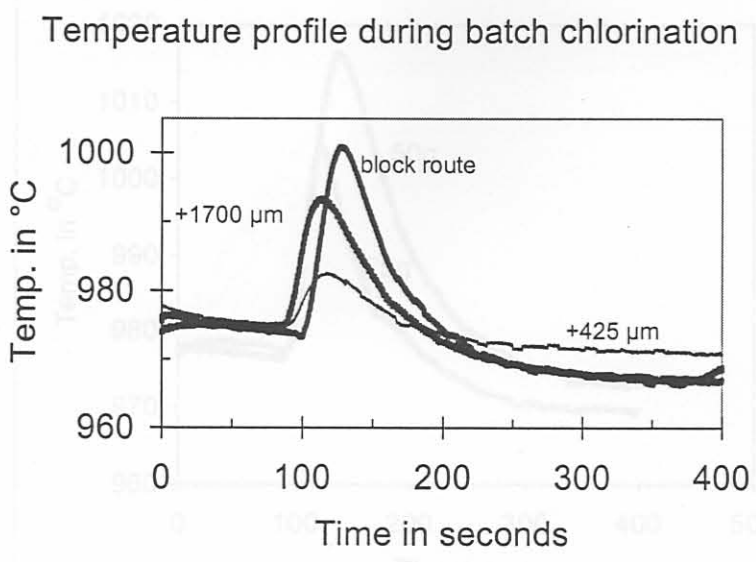

Figure 4.5b: Variation of the temperature change obtained for the initial chlorination of the three slag samples.

Experiments also showed that the temperature increase during the first few minutes of chlorination depended on the amount slag used for each chlorination run. Figure 4.5c shows that, the temperature change when 50g of slag was used was about 18% larger than when 25g of slag was used. This can be explained according to Pistorius and le Roux (2002) to be due to the balance of heat evolution in the volume of the sample with heat lost by radiation from the sample surface, Figure 4.5c.

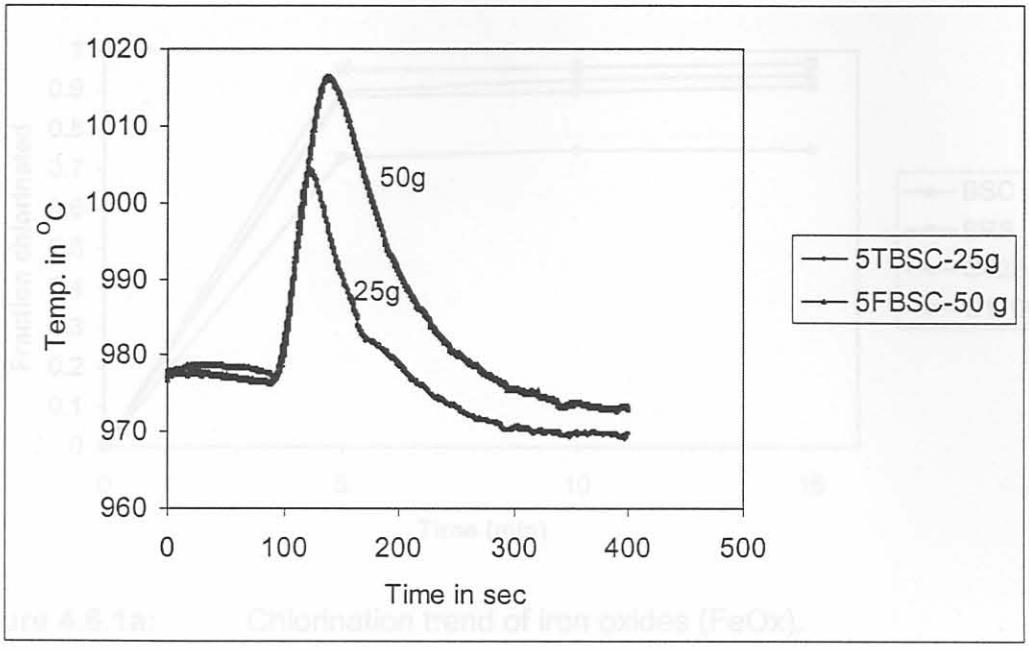

Figure 4.5c: Temperature profile showing the effect of sample mass on reaction exothermicity of the block route slag of the campaign (BSC).

4.6 Initial Rate Of Chlorination

4.6.1 Chlorination rate of FeOx and MnO.

The rate of chlorination of these oxides was comparatively high and the %chlorination of the oxides occured in the order granulated slag of size range 1700-2360μm > block route slags > slag of size range 425-600μm after the first five minutes of chlorination, figure 4.6.1.a and b.

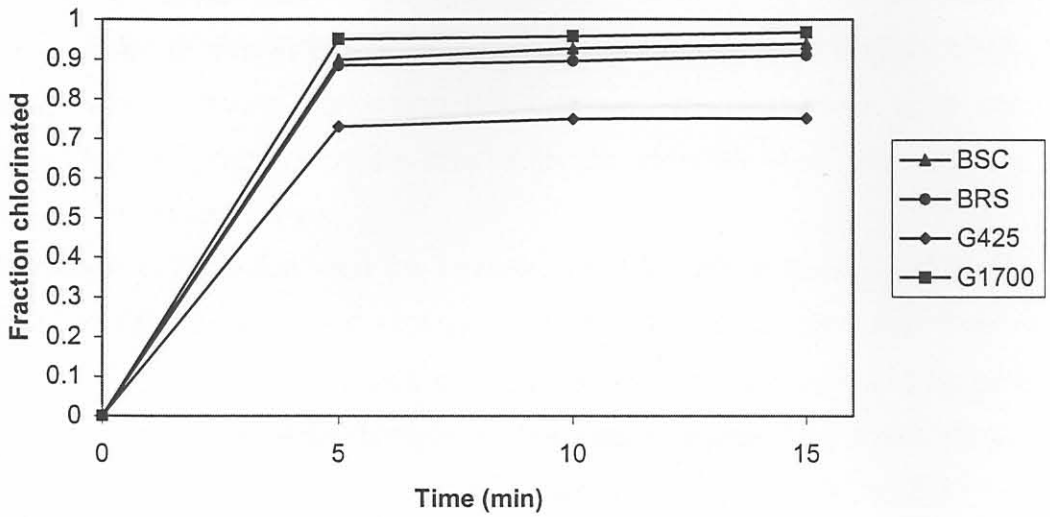

Figure 4.6.1a: Chlorination trend of iron oxides (FeOx).

The high chlorination rate of these oxides in the slag of size range 1700-2360μm could be attributed to the high porosity of the original slag which provides large surface area for the process. This was as compared to the block route slag which was relatively less porous making the initial chlorination of the oxide less rapid. The low rate of chlorination of these oxides in the slag of size range 425-600μm could be attributed firstly to the fact that, only part of the slag was relatively porous. The non-porous fraction locked some the oxides within the particle preventing them from being chlorinated. Secondly, as revealed by WDS analysis, during water granulation of the slag, almost all the Ti_2O_3 oxidized to TiO_2 while some of the Fe (II) oxides were oxidized to slower reacting Fe (III) oxides.

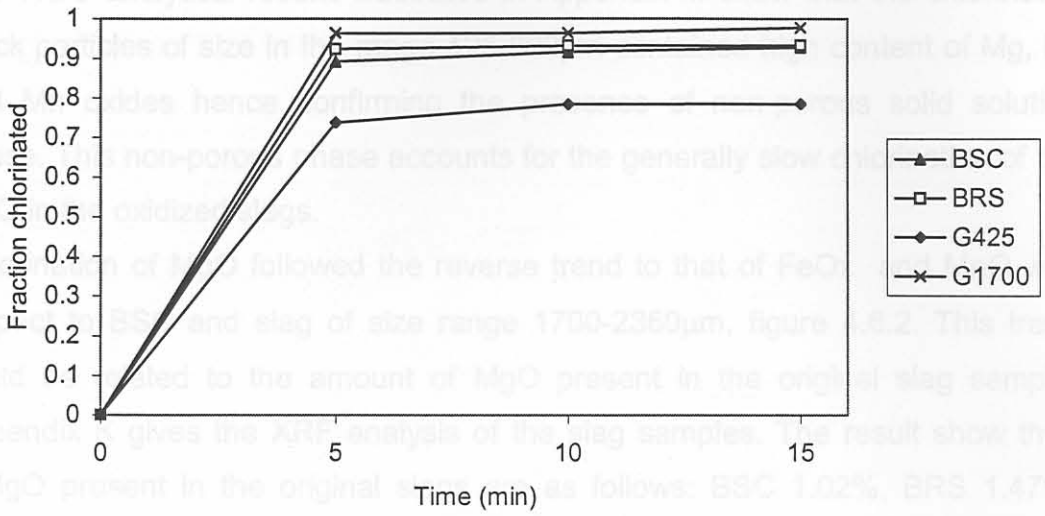

Figure 4.6.1b: Chlorination trend of manganese oxides (MnO).

4.6.2: Chlorination of MgO

As compared to the oxides, FeO and MnO, the chlorination of MgO was slower as only about 5-62% was chlorinated after 5 minutes. The general slow chlorination rate of the MgO phase was due to the association of the high boiling point liquid $MgCl_2$ with manganese and iron oxides forming a non porous phase.

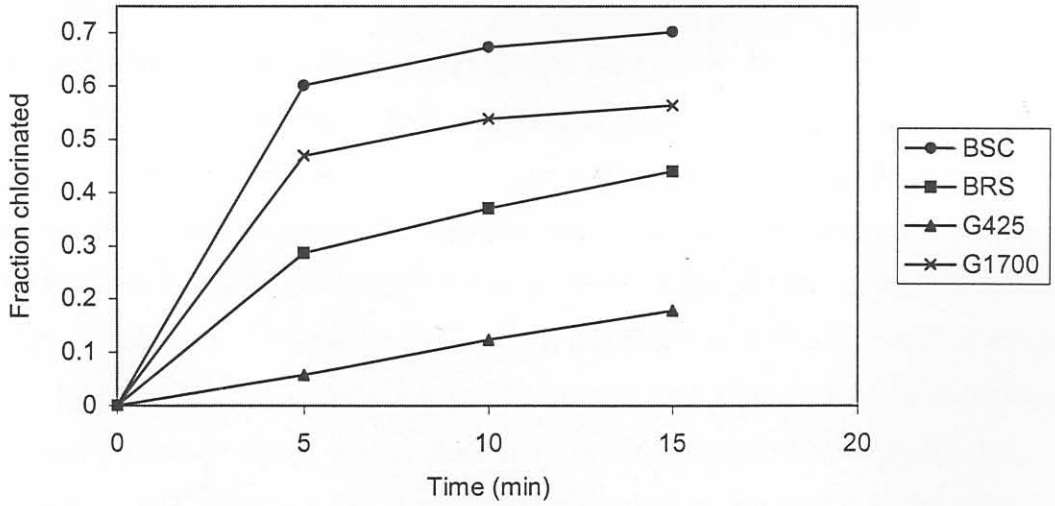

Figure 4.6.2: Chlorination trend of magnesium oxides

The WDS analytical results illustrated in Appendix M show that the chlorinated black particles of size in the range 425-600μm contained high content of Mg, Fe and Mn oxides hence confirming the presence of non-porous solid solution phase. This non-porous phase accounts for the generally slow chlorination of the MgO in the oxidized slags.

Chlorination of MgO followed the reverse trend to that of FeOx and MnO with respect to BSC and slag of size range 1700-2360μm, figure 4.6.2. This trend could be related to the amount of MgO present in the original slag sample. Appendix K gives the XRF analysis of the slag samples. The result show that, %MgO present in the original slags are as follows: BSC 1.02%, BRS 1.47%, G425-600μm 1.06%, G1700-2360μm 1.11%. The lowest content of MgO in BSC account for the highest chlorination rate of the slag as compared to BRS which contained the highest MgO content. The granulated slag of size range 425-600μm contained in addition to MgO, Fe (III) and Ti(IV) oxides accounting for the non-porous particles and the lowest chlorination rate observed.

Table 4.6: Summary of % chlorination of main oxides in titania slag after 5minutes.

Oxides	Slag type	% Chlorination after 5 minutes.
MnO	G+1700μm	96.39
"	BSC	89.25
"	G+425μm	73.74
"	BRS	92.40
FeO	G+1700μm	95.14
"	BSC	89.83
"	G+425μm	72.97
"	BRS	88.37
MgO	G+1700μm	46.93
"	BSC	60.10
"	G+425μm	5.79
"	BRS	28.68
TiO_2	G+425μm	2.14
"	G+1700μm	1.41
"	BSC	3.27
"	BRS	1.48

4.6.3: Chlorination of TiO_2.

As stated earlier the oxidation trend of the slags is in the order 425-600μm > 1700-2360μm > BSC > BRS. This implies that the percentage chlorination of the titanium dioxide in the slags are expected to decrease in the same order. This might be due to the decrease in porosity and the presence of higher magnesium oxide content in the highly oxidized slags. About 40% of the titanium present in block route slags is in the form Ti_2O_3 while the titanium in the granulated slag of size range 1700-2360μm was partially oxidized and that in slag of size range 425-600μm was completely oxidized. The highest chlorination rate of TiO_2 as exhibited by BSC (Figure 4.6.3) could be attributed to the fact that the slag was unoxidized and contain the lowest amount of MgO. This made it possible for

most of the FeO and MnO to be chlorinated within the first few minutes hence creating porosity in the slag particles which favours further chlorination.

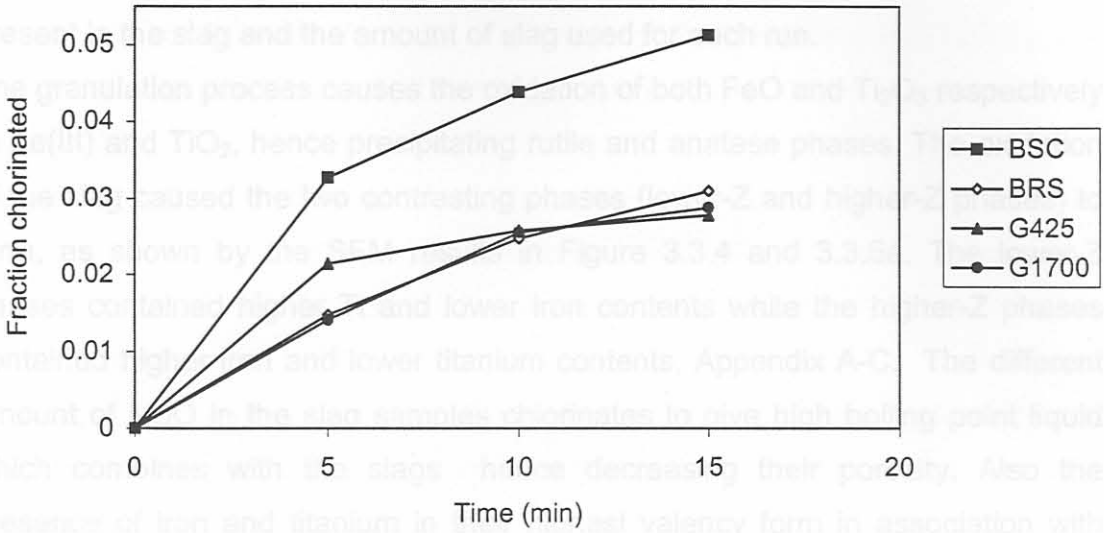

Figure 4.6.3: %Chlorination trend of Titanium dioxides

Comparing the two block route slags, 3.27%TiO_2 and 1.48%TiO_2 from BSC and BRS respectively were chlorinated within the first five minutes. This differences in chlorination rate of TiO_2 for the two block route slags could be attributed to the high MgO content of BRS, Appendix K.

The granulated slags on the other hand are oxidized and contained a relatively small amount of MgO as compared to BRS. Figure 4.6.3 shows that after 5 minutes of reaction time, the % chlorination of TiO_2 in the slag of size range 425-600μm and 1700-2360μm are given as 2.14% and 1.41% respectively. After about 15 minutes of chlorination, the %chlorination of TiO_2 for the typical block route slag (BRS) and the two granulated slags are comparable within experimental error. This show that there is no clear difference between the chlorination rate of block route and granulated slags. Further work, extended to longer chlorination times, would be required to clarify any differences.

5. References

Bergholm , A (1961). Chlorination *of Rutile, Transactions, American Institute of Mining Metallurgical and Petroleum Engineers*, Vol 221, pp1121-1129.

Bessinger, D; Geldenhuis, J. M. A; Pistorius, P. C; Mulaba, H.G (2001). *The decrepitation of solidified high titania slags, Journal of Non-Crystalline Solids*, vol. 282, pp132-142.

Bessinger, D; Du Plooy, H; Pistorius, P.C and Visser, C (1997). *Characteristics Of Some High Titania Slags, Heavy Minerals 1997. Proceedings Of A Conference Held In Durban, South Africa, South African Institute of Mining and Metallurgy,* pp 151-156.

Bonsack, J. P and Schneider, F. E (2001). *Entrained-Flow Chlorination of Titaniferous Slag to Produce Titanium Tetrachloride, Metallurgical and Materials Transactions B*, Vol 32B, pp 389-393.

Borowiec, K. T; Grau, A. E; Gueguin, M and Turgeon, J. F (1998). *Method of upgrade titania slag and resulting product, QIT-Fer Titane Inc., Quebec, Canada, U S Patent number 5, 830, 420*

Cole, S. S and Rowe, L. W (1962). Flash *Chlorination Of Very Finely Divided Metal Oxides. Transactions Of The American Institute of Mining and Engineering,* 224, pp 120-121.

Dunn, W. E Jr **(1960).** *High Temperature Chlorination of TiO_2 Bearing Minerals, Transaction; American Institute of Mining Metallurgical and Petroleum Engineers,* Vol 218, pp 6-12.

Eriksson, G and Pelton, A.D (1996). *Measurement and thermodynamic evaluation of phase equilibria in the Fe-Ti-O system. Berichteder. Bunsengesellschaft für physikalische Chemie.,* 100 (11), pp. 1839-1849.

Fisher, J. R (1997). *Developments in the TiO_2 pigments industry, which will drive demand for TiO_2 mineral feedstocks. Heavy Minerals, South African Institute of Mining and Metallurgy,* pp207-218.

GREY, I. E and Ward, J (1973). *An X-ray and Mössbauer study of the $FeTi_2O_5$-Ti_3O_5 system, Journal of Solid State Chemistry*, 7, pp 300-307.

Jeffrey, A. Kahn (1983) *Current Aspects on non-Rutile Titanium feedstocks, Light Metals, Metallurgical Society of the AIME*, pp1239-1241

Jena, P; Broccchi, E. A and Gameiro, D.H (1998). *Kinetics Of Chlorination Of TiO_2 By Cl_2 In The Presence Of Graphite Powder; Transactions of the Institution Mining Metallurgy*. 107, pp139-145.

Le Roux, J. T. F (2001). *Fluidized-bed Chlorination of Titania slag, Master degree thesis, University of Pretoria.*

Minkler, W. W and Baroch, E. F (1981). *The production of Titanium, Zirconium and Hafnium in J.K Tien and J.F Elliots (Eds), Metallurgical Treatises, Metallurgical Society of the AIME,* pp 171-182.

Morris, A. J and Jensen, R. F (1976). *Fluidized-Bed Chlorination Rates of Australian Rutile; Metallurgical Transactions B*, Vol.7B, pp89-93.

Nell, J (1999). *An Overview Of The Phase Chemistry Involved In The Production Of High-Titanium Slag From Ilmenite Feedstock; Heavy Minerals, South African Institute of Mining and Metallurgy,* pp137-145.

Noguchi, F. N; Ueda, T. Y (1980). *Australia/Japan Extractive Metallurgy Symposium, Sydney, Australia. Australian Institute of Mining and Metallurgy, Parkville, Victoria*, pp 479.

Pistorius, P.C and le Roux, J. T. F (2002). *Thermal, Chemical And Structural Changes During Initial Chlorination Of Titania Slag, Canadian Metallurgical quarterly,* vol.41, No 3, pp289-298.

Pistorius, P.C (2002). *The Relationship Between FeO And Ti_2O_3 In Ilmenite Smelter Slags; Scandinavian Journal Of Metallurgy*, 31, pp120-125.

Rao, Y. K. Chadwick, B. K (1988). *Chlorination of Rutile (TiO_2) with CO-Cl_2-He Gas Mixtures, Transactions of the Institution of Mining Metallurgy. Section.C,* Vol 97, pp167-179.

Reeves, J. W and Reeves, R. G (1997). *Misconceptions About Titanium Ore Chlorination. Heavy Minerals, Johannesburg, South African Institute Of Mining And Metallurgy*, pp. 203-206.

Rhee, K. I and Sohn, H. Y (1990). *The Selective Chlorination Of Iron From Ilmenite Ore By CO-Cl_2 Mixture: Part 1. Intrinsic Kinetics; Metallurgical Transactions B,* vol 21b, pp 321-330.

Richard Bay Minerals www.richards bay minerals.co.za/market.htm

Rowe, L. M and Opie, W. R (1955). *Production and Purification of $TiCl_4$. Journal Of Metals*, pp1189-1193.

Sigma-Aldrich www.sigma-aldrich.com

Sohn, H. Y and Zhou, L (1998). *The Kinetics of Carbochlorination of Titania Slag; The Canadian Journal of Chemical Engineering,* Vol 76, pp1078-1082.

Sohn, H. Y and Zhou, L (1999). *The Chlorination Kinetics Of Beneficiated Ilmenite Particles By Co and Cl_2 Mixtures; Chemical Engineering Journal,* Vol 72, pp37-42.

Stanaway. K. J. (1994). *Overview Of Titanium Dioxide Feedstock; Mining Engineering,* Vol 46, No 12 pp 1367-1370.

Szekely, J and Themelis, N. J (1971). *Rate Phenomena in Process Metallurgy, Wiley and sons, New York*, pp 639-650.

Teller, R. G; Antonio, M; Grau, A. E; Gueguin, M and Kostiner, E (1990). *Journal of Solid State Chemistry*, vol. 88, pp351-367.

Van Dyk, J. P, Visser, C. P and Vegter, N. M (1999). *Characteristic of various chlorinatable titaniferious product, Heavy Minerals, Johannesburg, South African Institute of Mining and Metallurgy*, pp153-157

Vasyutinsky, N. A (1968). *Kinetics and mechanism of the oxidation of a titanium slag, Russian Metallurgy,* vol. 4, pp29-34.

Vasyutinsky, N. A. and Movsesov, E. E (1965). Oxidation *and grinding of titanium slag, Russian Metallurgy*, vol. 4, pp56-57.

Zhou, L and Sohn, H. Y, Whiting, G. K and Leary, K. J (1996). *Microstructural Changes in Several Titaniferous Materials During Chlorination Reaction; Ind. Eng. Chem. Res.*, Vol 35, pp 954-962.

APPENDIX

Appendix A: Data for EDS analysis of different regions on the oxidized granulated slag sample of size range 106-425μm, in figure 3.3.4.

Part 1	Atom%	Mg	Al	Si	Ca	Ti	Mn	Fe
Ed dk	"	1.35	2.02	1.06	-	91.29	1.38	4.26
Ed lgt	"	3.44	4.28	7.17	0.42	62.33	3.89	16.94
Cendk	"	1.50	2.42	1.33	-	89.01	1.79	4.99
Cenlgt	"	2.41	2.92	2.58	-	79.69	2.29	10.10
Part 2								
Ed dk	"	-	1.72	1.27	-	95.37	-	2.27
Ed lgt	"	3.51	4. 43	5.36	-	66.99	3.65	16.06
Cendk	"	1.53	2.12	1.70	0.26	92.55	1.17	2.51
Cenlgt	"	3.12	4.39	6.30	0.47	67.04	3.57	14.77

Appendix B: Data for EDS analysis of different regions on the oxidized granulated slag sample of size range 1700-2360μm.

	Atom%	Mg	Al	Si	Ca	Ti	Mn	Fe
Part 1	"							
Ed dk	"	0.71	1.99	0.50	0.10	93.21	0.42	3.05
Ed lgt	"	1.78	3.47	4.95	0.56	73.61	2.92	11.70
Cen dk	"	0.45	1.58	0.73	0.00	94.18	0.59	2.49
Cen lgt	"	2.04	3.70	7.28	0.58	65.54	4.24	16.63
Part. 2	"	Mg	Al	Si	Ca	Ti	Mn	Fe
Ed dk	"	1.03	1.85	1.72	0.11	91.64	0.73	2.94
Ed lgt	"	3.30	3.87	2.89	0.41	76.37	2.97	10.24
Cen dk	"	0.48	1.87	0.54	0.04	92.96	0.59	3.42
Cen lgt	"	3.24	3.21	0.66	0.03	79.91	2.34	10.64

Appendix C: Data for EDS analysis of different regions on the oxidized granulated slag sample of size range > 4750μm, in figure 3.3.5.

Part 1	Atom%	Ti	Fe	Mn	Al	Si	Mg	Ca
Ed dk	"	92.95	2.93	0.23	1.97	1.02	0.79	0.12
Ed lgt	"	74.13	11.85	3.43	3.37	3.40	3.03	0.31
Cen dk	"	89.56	4.17	0.97	2.71	0.40	2.19	0.03
Cen lgt	"	75.54	12.48	2.84	3.62	3.20	1.99	0.35
Part 2								
Ed dk	"	93.69	2.95	0.26	1.92	0.54	0.57	0.09
Ed lgt	"	76.93	11.57	2.61	3.62	1.64	3.64	0.00
Cendk	"	87.75	5.31	1.17	2.66	0.45	2.64	0.04
Cenlgt	"	84.06	7.95	2.47	3.21	0.08	2.15	0.08
Part 3								
Ed dk	"	94.06	3.11	0.18	1.60	0.44	0.48	0.16
Ed lgt	"	77.86	11.11	2.79	3.34	2.27	2.47	0.16
Cendk	"	86.04	6.42	1.37	2.82	0.47	2.68	0.13
Cenlgt	"	73.02	12.75	3.68	3.10	4.48	2.30	0.39

Appendix D: EDS analysis of unoxidized block route slag, as in figure 3.3.6.

	Atom%	Mg	Al	Si	Ca	Ti	Mn	Fe
Part. 1								
Edge	"	3.56	1.51	0.00	0.00	75.80	1.54	17.60
Centre	"	3.93	1.22	0.00	0.00	78.19	"	16.66
Part. 2								
Edge	"	2.46	1.20	0.20	0.10	79.90	2.60	17.40
Centre	"	1.60	1.30	0.30	0.00	80.00	2.50	16.80

Appendix E1: EDS analysis of black particles of granulated slag of size range 425-600μm chlorinated for 15 minutes, as seen in figure 4.4.3a .

Pt1	Fe	Ti	Mn	Si	Mg	Al	Ca
Bk -Dk	5.90	87.00	1.20	2.10	1.80	1.40	0.60
Bk- Lt	18.70	66.70	2.40	3.80	5.30	2.90	0.30
P2;Bk-Dk	1.30	95.60	0.20	1.40	0.00	1.10	0.30
Bk-Lgt	25.70	53.60	3.30	6.80	6.30	3.50	0.90

Appendix E2: EDS analysis of light particles of granulated slag of size range 425-600μm chlorinated for 15 minutes, as seen in figure 4.4.3c

Pt1	Fe	Ti	Mn	Si	Mg	Al	Ca
Lgt –Ed	0.10	97.50	0.10	1.10	0.40	0.60	0.20
Lgt- Cen	1.40	92.40	0.10	0.50	3.60	1.90	0.10
Pt 2;Lt-Ed	0.00	97.60	0.00	1.20	0.10	0.90	0.20
Lgt-Cen	0.60	97.70	0.20	0.20	0.50	0.70	0.10
Pt3;Lt-Ed	0.30	98.90	0.10	0.30	0.10	0.20	0.10
Lgt-Cen	1.50	92.70	0.00	0.80	3.40	1.40	0.10

Appendix E3: EDS Analysis of granulated slag of size range 1700-2360μm chlorinated for 15 minutes, as seen in figure 4.4.3d

Pt1	Fe	Ti	Mn	Si	Mg	Al	Ca
Lgt –Ed	0.00	97.00	0.10	1.80	0.30	0.60	0.20
Lgt- Cen	0.30	97.30	0.00	0.20	1.40	0.70	0.10
Pt 2;Lt-Ed	0.00	94.10	0.10	2.50	1.40	1.60	0.30
Lgt-Cen	0.10	97.80	0.00	0.40	0.70	0.80	0.20
Pt3;Lt-Ed	0.10	96.60	0.00	1.80	0.30	0.70	0.50
Lgt-Cen	0.00	97.40	0.00	0.40	1.20	0.90	0.20

Appendix E4: EDS analysis of block route slag chlorinated for 5 minutes, as seen in figure 4.4.3e

Pt1	Fe	Ti	Mn	Si	Mg	Al	Ca
Brs –Ed	0.10	98.20	0.00	1.00	0.20	0.40	0.00
Brs – Cen	1.40	87.70	0.10	0.30	0.10	0.50	0.30
Pt2;Bs-Ed	0.10	98.90	0.00	0.30	5.70	1.80	0.20
Brs –Cen	3.60	85.60	0.50	0.40	7.80	2.20	0.00
Pt3;Bs-Ed	0.20	98.30	0.00	0.50	0.30	0.60	0.20
Brs –Cen	7.70	86.50	0.50	0.20	3.00	2.00	0.10

Appendix F: XRD spectra showing the prominent peak at 28.74^{O} corresponding to an iron titanium oxide solid solution in granulated slag of size range 600-1180μm.

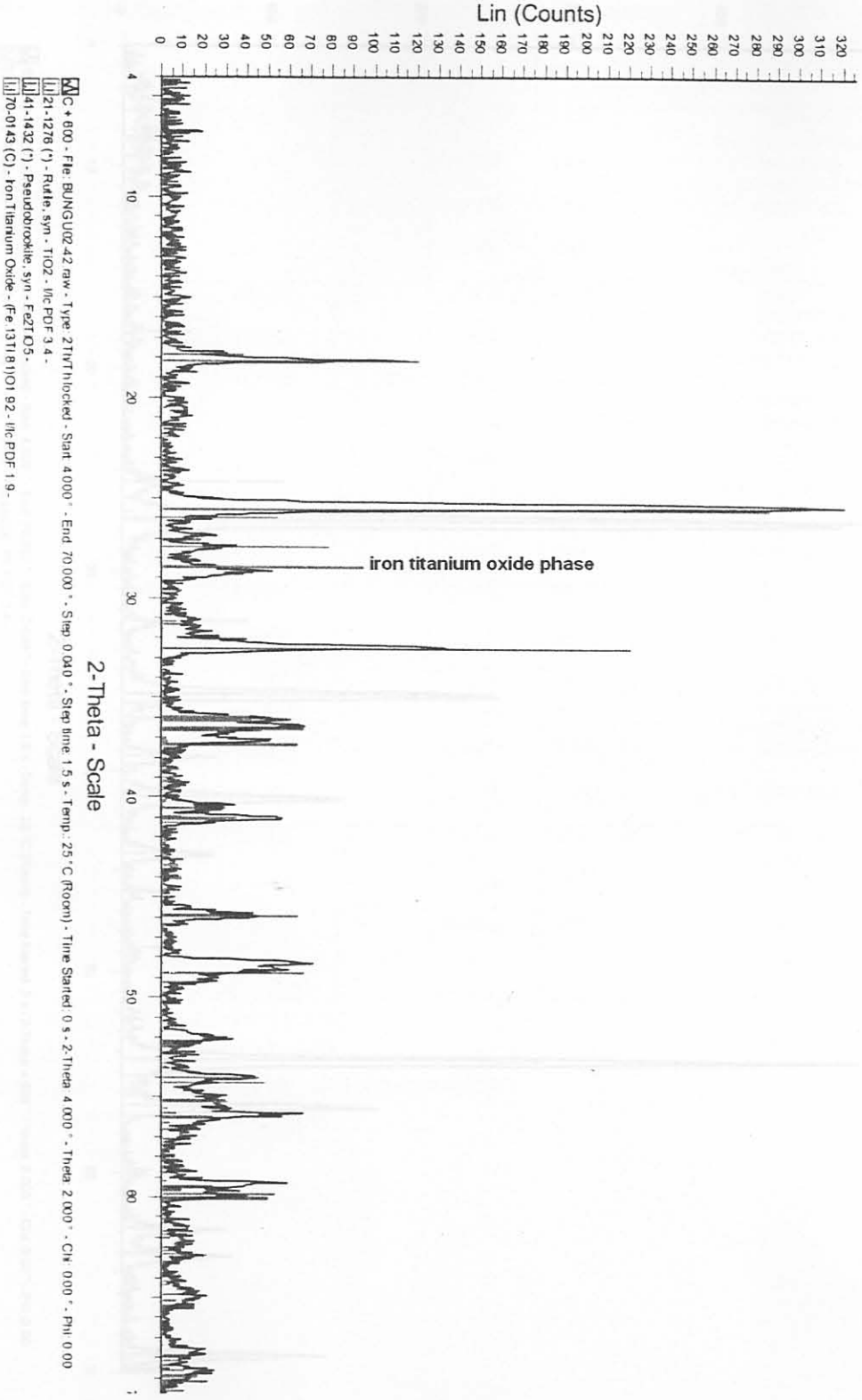

Appendix G: XRD spectra showing the phases present in granulated titania slag of size range 425 - 600μm chlorinated for 15 minutes .

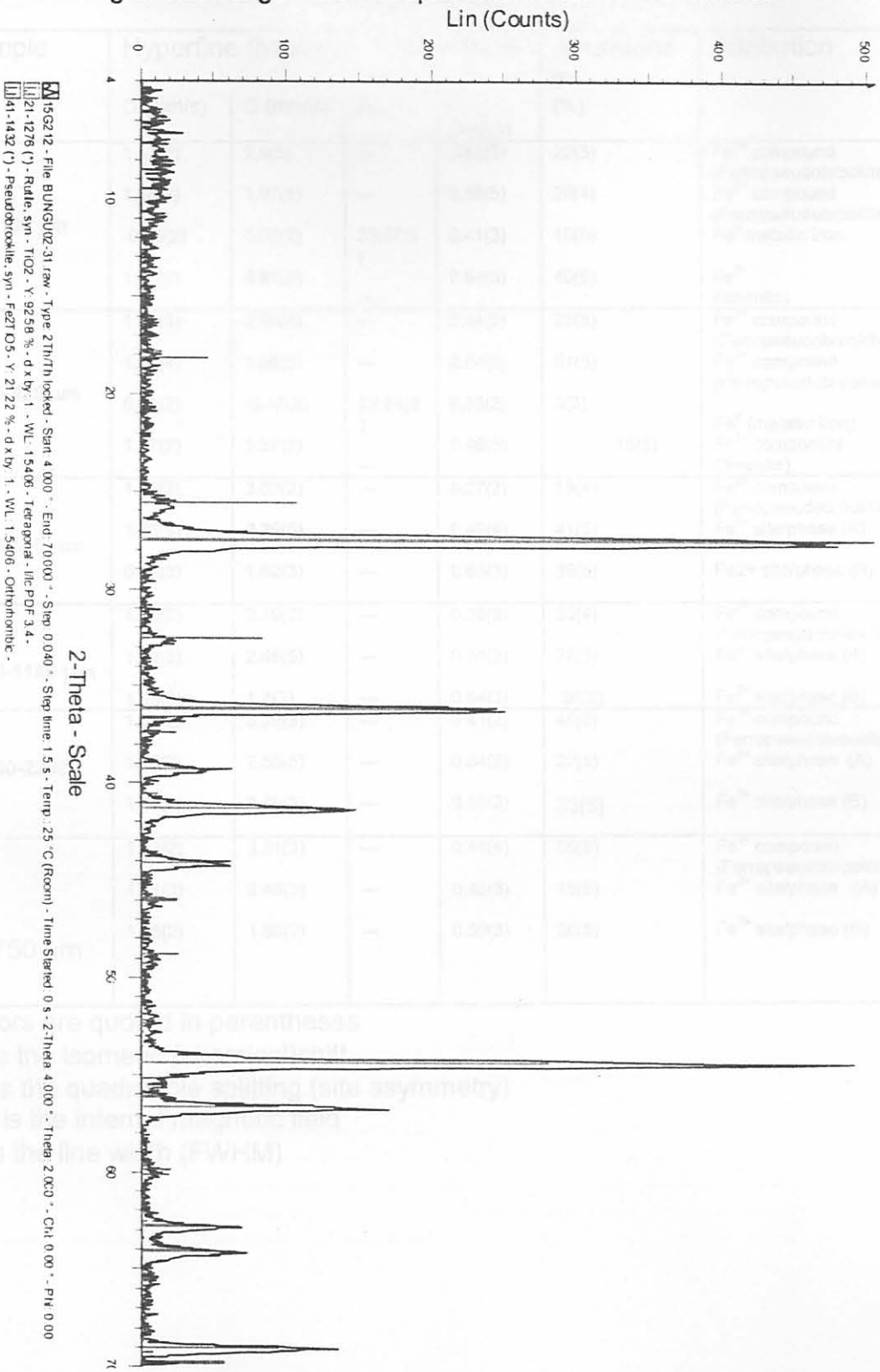

Appendix H: Hyperfine interaction parameters of the different size ranges of granulated slag (Mössbauer analysis).

Sample	Hyperfine Interaction Parameters				Abundance (%)	Attribution
	□ (mm/s)	□ (mm/s)	B_{hf} (T)	□ (mm/s)		
+75-106 μm	1.13(2)	2.9(5)	---	0.45(3)	22(5)	Fe^{2+} compound (Ferropseudobrookite, site-1)
	1.06(3)	1.97(5)	---	0.58(5)	28(4)	Fe^{2+} compound (Ferropseudobrookite, site-2)
	-0.45(2)	0.02(2)	33.57(5)	0.41(3)	10(5)	Fe^{0} metallic iron
	1.05(3)	0.81(2)	---	0.54(3)	40(5)	Fe^{2+} (Ilmenite)
+106-425 μm	1.09(3)	2.95(4)	---	0.44(2)	28(5)	Fe^{2+} compound (Ferropseudobrookite,site-1)
	1.04(4)	1.99(5)	---	0.64(3)	51(5)	Fe^{2+} compound (Ferropseudobrookite, site-2)
	0.00(2)	-0.17(3)	32.54(5)	0.33(3)	3(3)	Fe^{0} (metallic iron)
	1.07(2)	0.87(3)	---	0.46(5)	18(5)	Fe^{2+} component (Ilmenite)
+425-600 μm	1.09(2)	3.03(2)	---	0.27(3)	19(4)	Fe^{2+} compound (Ferropseudobrookite site-1)
	1.00(3)	2.39(5)	---	0.49(4)	41(5)	Fe^{2+} site/phase (A)
	0.99(3)	1.62(3)	---	0.60(3)	39(5)	Fe2+ site/phase (B)
+600-1180 μm	1.13(2)	3.19(2)	---	0.36(3)	36(4)	Fe^{2+} compound (Ferropseudobrookite site-1)
	1.12(3)	2.46(5)	---	0.51(3)	28(5)	Fe^{2+} site/phase (A)
	1.09(3)	1.7(3)	---	0.64(3)	36(3)	Fe^{2+} site/phase (B)
+1700-2360 μm	1.18(2)	3.29(3)	---	0.41(2)	45(5)	Fe^{2+} compound (Ferropseudobrookite site-1)
	1.16(3)	2.55(5)	---	0.54(3)	22(5)	Fe^{2+} site/phase (A)
	1.14(3)	1.89(3)	---	0.59(3)	33(5)	Fe^{2+} site/phase (B)
+4750 μm	1.18(2)	3.31(3)	---	0.44(4)	55(5)	Fe^{2+} compound (Ferropseudobrookite site-1)
	1.01(3)	2.46(3)	---	0.43(3)	15(5)	Fe^{2+} site/phase (A)
	1.15(2)	1.85(2)	---	0.59(3)	30(5)	Fe^{2+} site/phase (B)

Errors are quoted in parentheses
δ is the isomeric (chemical)shift
Δ is the quadrupole splitting (site asymmetry)
B_{hf} is the internal magnetic field
Γ is the line width (FWHM)

Appendix I: Chlorination parameters and results obtained.

Minimum fluidization velocity = 5.7l/min
Maximum fluidization velocity = 17.84l/min
Atmospheric pressure =86kPa
Total pressure that could be tolerated = 108-115 kPa at a flowrate of 16.5l/min at 22.5^{O}C
Reaction temperature = 1000 ^{O}C
Particle size range used: 425 - 600μm.

Gas mixture used :

Rotameter reading	Gas	Flowrate(l/min)	%
100	CO	2.75	20.75
20	Cl_2	4.00	30.19
30	N_2	6.50	49.06
Total		13.25	100.00

EXPT 1

Block route slag (BRS)

Name of sample	5BRS
Mass of sample(g)	25.02
Room temperature(^{O}C)	20.00
Reaction pressure(kPa)	89.06
Reaction time(mins)	5.00
Mass of product(g)	21.49
Reduction in mass(g)	3.53
Name of sample	10BRS
Mass of sample(g)	25.00
Room temperature(^{O}C)	21.00
Reaction pressure(kPa)	89.32
Reaction time(mins)	10.00
Mass of product(g)	21.25
Reduction in mass(g)	3.76
Name of sample	15BRS
Mass of sample(g)	25.00
Room temperature(^{O}C)	20.00
Reaction pressure(kPa)	112.05
Reaction time(mins)	15.00
Mass of product(g)	21.00
Reduction in mass(g)	4.00

EXPT 2

Block route slag of the campaign (BSC)

Name of sample	5BSC
Mass of sample(g)	25.00
Room temperature(^{O}C)	22.00
Reaction pressure(kPa)	90.92
Reaction time(mins)	5.00
Mass of product(g)	21.65
Reduction in mass(g)	3.35
Name of sample	10BSC
Mass of sample(g)	25.00
Room temperature(^{O}C)	22.00
Reaction pressure(kPa)	89.46
Reaction time(mins)	10.00
Mass of product(g)	21.34
Reduction in mass(g)	3.66
Name of sample	15BSC
Mass of sample(g)	25.00
Room temperature(^{O}C)	21.00
Reaction pressure(kPa)	88.52
Reaction time(mins)	15.00
Mass of product(g)	21.15
Reduction in mass(g)	3.85
Name of sample	20BSC
Mass of sample(g)	25.00
Room temperature(^{O}C)	21.00
Reaction pressure(kPa)	91.00
Reaction time(mins)	20.00
Mass of product(g)	20.75
Reduction in mass(g)	4.25

EXPT 3

Granulated slag of size range 1700 - 2360μm

A

Name of sample	5C1700
Mass of sample(g)	25.01
Room temperature(^{O}C)	20.50
Reaction pressure(kPa)	89.46
Reaction time(mins)	5.00
Mass of product(g)	22.32
Reduction in mass(g)	2.69
Name of sample	10C1700
Mass of sample(g)	25.01
Room temperature(^{O}C)	19.50
Reaction pressure(kPa)	88.79
Reaction time(mins)	10.00
Mass of product(g)	22.09
Reduction in mass(g)	2.92
Name of sample	15C1700
Mass of sample(g)	25.01
Room temperature(^{O}C)	21.00
Reaction pressure(kPa)	88.26
Reaction time(mins)	15.00
Mass of product(g)	22.00
Reduction in mass(g)	3.00

B

Name of sample	5C1700
Mass of sample(g)	25.02
Room temperature(^{O}C)	26.00
Reaction pressure(kPa)	102.00
Reaction time(mins)	5.00
Mass of product(g)	22.38
Reduction in mass(g)	2.64
Name of sample	10C1700
Mass of sample(g)	25.04
Room temperature(^{O}C)	26.20
Reaction pressure(kPa)	101.00
Reaction time(mins)	10.00
Mass of product(g)	22.24
Reduction in mass(g)	2.80
Name of sample	15C1700
Mass of sample(g)	25.00
Room temperature(^{O}C)	26.00
Reaction pressure(kPa)	140.00
Reaction time(mins)	15.00
Mass of product(g)	22.00
Reduction in mass(g)	3.00

EXPT 4	
Granulated slag of size range 425 - 600μm	
A	
Name of sample	5C425
Mass of sample(g)	25.03
Room temperature(^{O}C)	24.00
Reaction pressure(kPa)	101.00
Reaction time(mins)	5.00
Mass of product(g)	22.88
Reduction in mass(g)	2.16
Name of sample	10C425
Mass of sample(g)	25.00
Room temperature(^{O}C)	27.00
Reaction pressure(kPa)	113.00
Reaction time(mins)	10.00
Mass of product(g)	22.73
Reduction in mass(g)	2.28
Name of sample	15C425
Mass of sample(g)	25.00
Room temperature(^{O}C)	27.00
Reaction pressure(kPa)	120.00
Reaction time(mins)	15.00
Mass of product(g)	22.07
Reduction in mass(g)	2.93

B	
Name of sample	5C425
Mass of sample(g)	25.02
Room temperature(^{O}C)	24.90
Reaction pressure(kPa)	100.00
Reaction time(mins)	5.00
Mass of product(g)	22.86
Reduction in mass(g)	2.15
Name of sample	10C425
Mass of sample(g)	25.03
Room temperature(^{O}C)	27.00
Reaction pressure(kPa)	100.00
Reaction time(mins)	10.00
Mass of product(g)	22.32
Reduction in mass(g)	2.71
Name of sample	15C425
Mass of sample(g)	25.00
Room temperature(^{O}C)	27.00
Reaction pressure(kPa)	114.00
Reaction time(mins)	15.00
Mass of product(g)	22.09
Reduction in mass(g)	2.91

C	
Name of sample	5C425
Mass of sample(g)	25.00
Room temperature(^{O}C)	27.00
Reaction pressure(kPa)	101.00
Reaction time(mins)	5.00
Mass of product(g)	22.08
Reduction in mass(g)	2.92
Name of sample	10C425
Mass of sample(g)	25.01
Room temperature(^{O}C)	27.00
Reaction pressure(kPa)	101.00
Reaction time(mins)	10.00
Mass of product(g)	22.53
Reduction in mass(g)	2.48
Name of sample	15C425
Mass of sample(g)	25.01
Room temperature(^{O}C)	25.00
Reaction pressure(kPa)	15.00
Reaction time(mins)	99.00
Mass of product(g)	21.98
Reduction in mass(g)	3.03

D	
Name of sample	5C425
Mass of sample(g)	25.01
Room temperature(^{O}C)	27.00
Reaction pressure(kPa)	133.00
Reaction time(mins)	5.00
Mass of product(g)	22.49
Reduction in mass(g)	2.52
Name of sample	10C425
Mass of sample(g)	25.01
Room temperature(^{O}C)	27.00
Reaction pressure(kPa)	100.00
Reaction time(mins)	10.00
Mass of product(g)	22.64
Reduction in mass(g)	2.37
Name of sample	15C425
Mass of sample(g)	25.01
Room temperature(^{O}C)	27.50
Reaction pressure(kPa)	101.00
Reaction time(mins)	15.00
Mass of product(g)	21.77
Reduction in mass(g)	3.24

Appendix J: Calibration curves of the three gases used during chlorination.

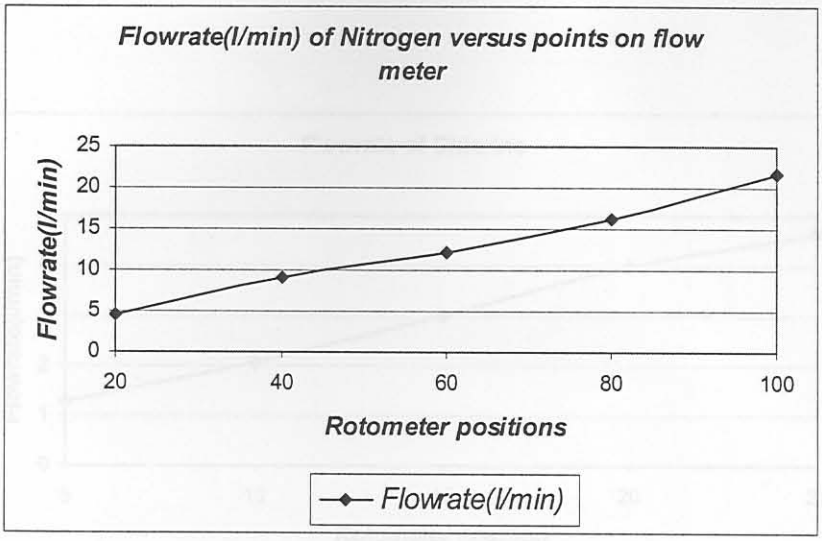

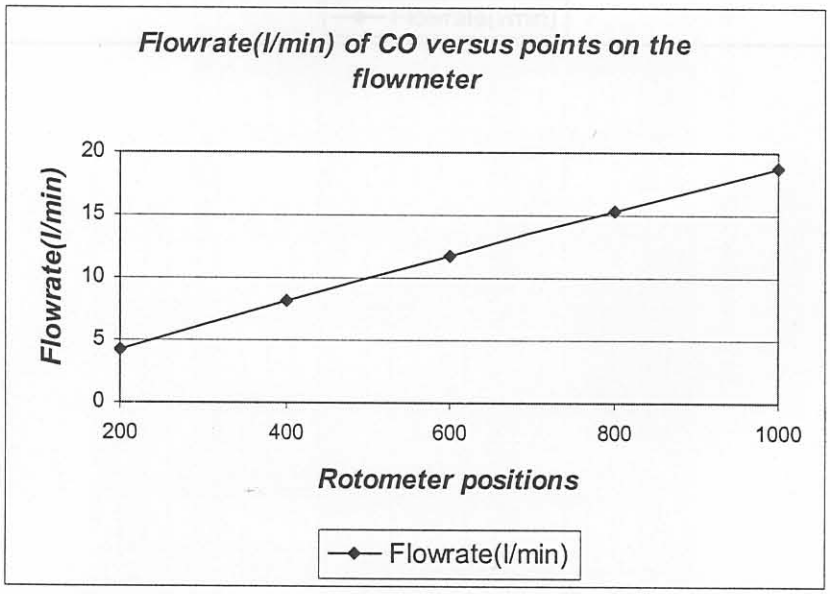

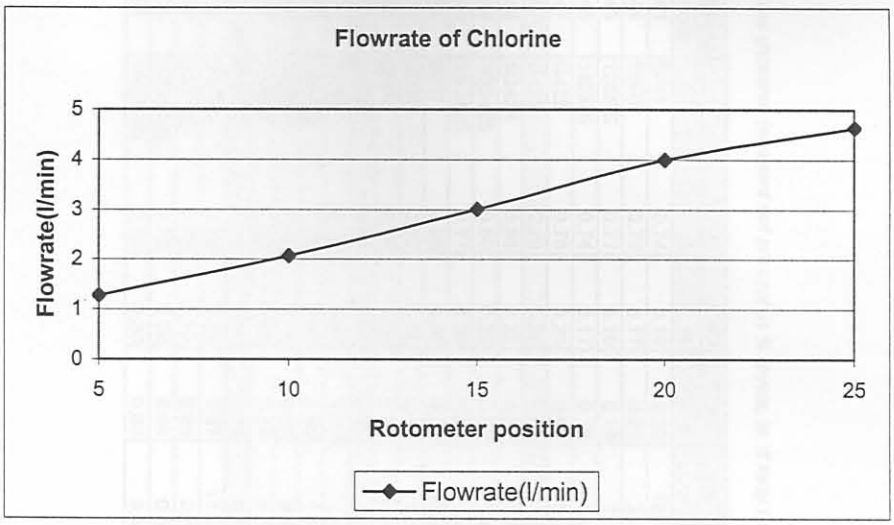

Appendix K: XRF analysis of both the chlorinated and unchlorinated slag samples

*nd: not detected (element not present in % levels, ie. It may be absent or present in trace amounts)

Reference number		Al2O3 %	CaO %	Cr2O3 %	Fe2O3t %	K2O %	MgO %	MnO %	Na2O %	P2O5 %	SiO2 %	TiO2 %	V2O5 %	Zr2O %	Total %
DB443	BRS	0.74	0.19	0.20	16.99	nd	1.47	1.13	nd	nd	1.21	81.37	0.45	0.20	103.95
DB444	5BRS	0.79	0.17	0.21	2.30	nd	1.22	0.10	nd	nd	1.39	93.29	0.11	0.24	99.84
DB445	10BRS	0.77	0.19	0.19	2.10	nd	1.09	0.09	nd	nd	1.49	93.39	0.09	0.25	99.65
DB446	15BRS	0.74	0.17	0.18	1.79	nd	0.98	0.09	nd	nd	1.45	93.90	0.08	0.25	99.61
DB447	G425	0.75	0.20	0.07	11.22	nd	1.06	1.21	nd	nd	1.28	85.04	0.46	0.22	101.52
DB447QC	G425	0.76	0.20	0.07	11.21	nd	1.12	1.21	nd	nd	1.26	85.47	0.46	0.23	102.00
DB448	5G425	0.85	0.22	0.07	2.31	nd	1.06	0.18	nd	nd	1.51	92.96	0.12	0.25	99.53
DB449	10G425	0.80	0.22	0.06	1.97	nd	0.88	0.17	nd	nd	1.47	93.72	0.10	0.25	99.64
DB450	15G425	0.77	0.20	0.05	1.64	nd	0.66	0.16	nd	nd	1.50	94.43	0.08	0.25	99.73
DB451	BSC	0.98	0.08	0.11	13.62	nd	1.02	1.53	nd	nd	1.04	85.13	0.44	0.15	104.11
DB452	1BSC	0.92	0.06	0.10	1.89	nd	0.57	0.22	nd	nd	1.24	94.53	0.11	0.18	99.82
DB453	2BSC	0.86	0.06	0.09	1.68	nd	0.45	0.19	nd	nd	1.22	94.83	0.08	0.18	99.65
DB453QC	2BSC	0.88	0.07	0.09	1.68	nd	0.50	0.20	nd	nd	1.29	95.00	0.08	0.18	99.96
DB454	5BSC	0.86	0.07	0.07	1.60	nd	0.47	0.19	nd	nd	1.30	95.09	0.08	0.19	99.91
DB455	10BSC	0.78	0.06	0.06	1.17	nd	0.39	0.15	nd	nd	1.20	95.36	0.06	0.18	99.39
DB456	15BSC	0.83	0.08	0.07	0.96	nd	0.36	0.13	nd	nd	1.48	95.47	0.04	0.19	99.60
DB457	20BSC	0.81	0.08	0.04	0.75	nd	0.30	0.08	nd	nd	1.49	96.15	0.03	0.19	99.92
DB457QC	20BSC	0.80	0.07	0.04	0.75	nd	0.26	0.07	nd	nd	1.41	96.28	0.03	0.19	99.90
DB458	G1700	0.79	0.20	0.07	11.21	nd	1.11	1.22	nd	nd	1.38	86.66	0.47	0.22	103.34
DB459	5G1700	0.77	0.19	0.05	0.61	nd	0.66	0.05	nd	nd	1.57	95.72	0.06	0.26	99.94
DB460	10G1700	0.72	0.20	0.04	0.54	nd	0.58	0.05	nd	nd	1.54	95.61	0.04	0.25	99.57
DB461	15G1700	0.73	0.20	0.03	0.41	nd	0.55	0.03	nd	nd	1.58	95.66	0.03	0.25	99.47

APPENDIX M: Composition of various phases in titania slags (in wt%). Fe, Mn, O, Ti, and V by WDS, other elements by EDS;

C4346 – Chlorinated black particles of size 425-600 μm,

C4349 – FeO-containing rutile in unchlorinated slag of size 425 - 600μm

C4350 – FeO-containing rutile in unchlorinated slag of size 2360 - 3350 μm

No.	Al	Ca	Fe	Mg	Mn	O	Si	Ti	V	Total	Label
3	0.50	0.00	2.00	0.20	0.20	39.20	0.10	58.20	0.00	100.40	C4350 P001
4	0.40	0.00	1.70	0.10	0.20	38.40	0.10	58.00	0.00	98.90	C4350 P002
5	0.90	0.00	2.90	0.80	0.40	36.00	0.10	58.20	0.20	99.50	C4350 P003
6	1.00	0.00	3.50	0.80	0.50	35.30	0.10	57.40	0.10	98.70	C4350 P004
8	0.30	0.00	2.00	0.10	0.30	38.60	0.20	57.70	0.00	99.20	C4350 P006
9	0.30	0.00	1.90	0.00	0.30	38.30	0.10	58.30	0.00	99.20	C4350 P007
10	0.40	0.00	1.70	0.10	0.20	38.30	0.10	58.30	0.00	99.10	C4350 P008
11	0.40	0.00	1.80	0.10	0.20	38.80	0.20	58.30	0.10	99.90	C4350 P009
12	0.40	0.00	2.00	0.10	0.30	38.20	0.10	57.80	0.00	98.90	C4350 P010
13	0.40	0.10	1.70	0.10	0.20	39.10	0.10	58.40	0.00	100.10	C4350 P011
14	0.40	0.00	1.70	0.10	0.30	39.10	0.10	57.80	0.00	99.50	C4350 P012
18	0.30	0.00	25.50	2.50	3.50	36.50	0.10	33.10	0.10	101.60	C4346 P015
20	0.60	0.00	22.40	2.40	2.40	36.30	0.10	36.10	0.20	100.50	C4346 P017
21	0.40	0.10	22.40	2.40	3.90	36.50	0.40	34.50	0.30	100.90	C4346 P018
22	0.60	0.00	22.00	2.30	3.50	36.60	0.20	36.00	0.20	101.40	C4346 P019
23	0.40	0.00	16.20	2.60	2.50	40.30	0.20	42.30	0.10	104.60	C4346 P020
24	0.80	0.10	22.10	2.20	3.10	36.60	0.80	33.70	0.10	99.50	C4346 P021
25	0.90	0.10	22.80	2.20	2.90	37.40	0.90	33.90	0.20	101.30	C4346 P022
26	1.00	0.30	19.20	2.00	2.40	39.20	1.10	37.80	0.10	103.10	C4346 P023
27	0.70	0.10	19.30	2.00	2.90	38.30	0.50	38.00	0.30	102.10	C4346 P024
28	1.00	0.10	25.20	1.70	1.90	40.30	0.40	34.70	0.00	105.30	C4346 P025
29	0.10	0.00	0.20	0.00	0.00	40.20	0.10	59.10	0.00	99.70	C4346 P026
30	0.50	0.00	1.50	0.20	0.20	38.20	0.10	58.40	0.20	99.30	C4349 P027
31	0.60	0.00	2.00	0.20	0.30	38.30	0.10	57.90	0.50	99.90	C4349 P028